

ARTICLE

# Impaired respiratory burst contributes to infections in PKC $\delta$ -deficient patients

Anna-Lena Neehus<sup>1,2,3</sup> , Kunihiro Moriya<sup>1,2\*</sup> , Alejandro Nieto-Patlán<sup>1,2,4,5\*</sup> , Tom Le Voyer<sup>1,2</sup> , Romain Lévy<sup>1,2,6</sup> , Ahmet Özen<sup>7</sup> , Elif Karakoc-Aydiner<sup>7</sup> , Safa Baris<sup>7</sup> , Alisan Yildiran<sup>8</sup> , Engin Altundag<sup>9</sup> , Manon Roynard<sup>1,2</sup> , Kathrin Haake<sup>3</sup> , Mélanie Migaud<sup>1,2</sup> , Karim Dorgham<sup>10</sup> , Guy Gorochov<sup>10</sup> , Laurent Abel<sup>1,2,11</sup> , Nico Lachmann<sup>3</sup> , Figen Dogu<sup>12\*\*</sup> , Sule Haskologlu<sup>12\*\*</sup> , Erdal İnce<sup>13\*\*</sup> , Jamel El-Benna<sup>14,15\*\*</sup> , Gulbu Uzel<sup>16\*\*</sup> , Ayca Kiykim<sup>17,18\*\*</sup> , Kaan Boztug<sup>19,20,21,22\*\*</sup> , Marion R. Roderick<sup>23\*\*</sup> , Mohammad Shahrooei<sup>24,25\*\*</sup> , Paul A. Brogan<sup>26\*\*</sup> , Hassan Abolhassani<sup>27,28\*\*</sup> , Gonca Hancioglu<sup>8\*\*</sup> , Nima Parvaneh<sup>29,30\*\*</sup> , Alexandre Belot<sup>31\*\*</sup> , Aydan Ikinciogullari<sup>12\*\*</sup> , Jean-Laurent Casanova<sup>1,2,11,32\*\*\*</sup> , Anne Puel<sup>1,2,11\*\*\*</sup> , and Jacinta Bustamante<sup>1,2,11,33\*\*\*</sup> 

**Patients with autosomal recessive protein kinase C  $\delta$  (PKC $\delta$ ) deficiency suffer from childhood-onset autoimmunity, including systemic lupus erythematosus. They also suffer from recurrent infections that overlap with those seen in patients with chronic granulomatous disease (CGD), a disease caused by defects of the phagocyte NADPH oxidase and a lack of reactive oxygen species (ROS) production. We studied an international cohort of 17 PKC $\delta$ -deficient patients and found that their EBV-B cells and monocyte-derived phagocytes produced only small amounts of ROS and did not phosphorylate p40<sup>p<sub>Hox</sub></sup> normally after PMA or opsonized *Staphylococcus aureus* stimulation. Moreover, the patients' circulating phagocytes displayed abnormally low levels of ROS production and markedly reduced neutrophil extracellular trap formation, altogether suggesting a role for PKC $\delta$  in activation of the NADPH oxidase complex. Our findings thus show that patients with PKC $\delta$  deficiency have impaired NADPH oxidase activity in various myeloid subsets, which may contribute to their CGD-like infectious phenotype.**

<sup>1</sup>Laboratory of Human Genetics of Infectious Diseases, Necker Branch, Institut National de la Santé et de la Recherche Médicale UMR 1163, Paris, France; <sup>2</sup>University of Paris, Imagine Institute, Paris, France; <sup>3</sup>Institute of Experimental Hematology, REBIRTH Research Center for Translational and Regenerative Medicine, Hannover Medical School, Hannover, Germany; <sup>4</sup>Research and Development in Bioprocess Unit, National School of Biological Sciences, National Polytechnic Institute, Mexico City, Mexico; <sup>5</sup>National Laboratory for Specialized Services of Investigation, Development and Innovation for Pharma Chemicals and Biotechnological Products, LANSEIDI-FarBiotec-CONACyT, Mexico City, Mexico; <sup>6</sup>Pediatric Hematology-Immunology Unit, Necker Hospital for Sick Children, Paris, France; <sup>7</sup>Department of Pediatrics, Division of Allergy and Immunology, Marmara University, School of Medicine, Istanbul, Turkey; <sup>8</sup>Department of Pediatric Immunology and Allergy, Ondokuz Mayıs University School of Medicine, Samsun, Turkey; <sup>9</sup>Department of Medical Genetics, Ondokuz Mayıs University Faculty of Medicine, Samsun, Turkey; <sup>10</sup>Sorbonne University, Institut National de la Santé et de la Recherche Médicale, Center for Immunology and Microbial Infections, CIMI-Paris, Assistance Publique-Hôpitaux de Paris, Pitié-Salpêtrière Hospital, Department of Immunology, Paris, France; <sup>11</sup>St. Giles Laboratory of Human Genetics of Infectious Diseases, Rockefeller Branch, The Rockefeller University, New York, NY; <sup>12</sup>Department of Pediatric Immunology and Allergy, Ankara University School of Medicine, Ankara, Turkey; <sup>13</sup>Department of Pediatric Infectious Disease, Ankara University School of Medicine, Ankara, Turkey; <sup>14</sup>University of Paris, Institut National de la Santé et de la Recherche Médicale U1149, Centre National de la Recherche Scientifique-ERL8252, Paris, France; <sup>15</sup>Center for Research on Inflammation, Laboratory of Excellence Inflammex, Faculty of Medicine, Xavier Bichat, Paris, France; <sup>16</sup>Laboratory of Clinical Infectious Diseases, National Institute of Allergy and Infectious Diseases, National Institutes of Health, Bethesda, MD; <sup>17</sup>Pediatric Allergy and Immunology, Marmara University Pediatric Training and Research Hospital, Istanbul, Turkey; <sup>18</sup>Division of Pediatric Allergy and Immunology, Cerrahpasa School of Medicine, Istanbul University-Cerrahpasa, Istanbul, Turkey; <sup>19</sup>CeMM Research Center for Molecular Medicine of the Austrian Academy of Sciences, Vienna, Austria; <sup>20</sup>St. Anna Children's Hospital, Department of Pediatrics and Adolescent Medicine, Medical University of Vienna, Vienna, Austria; <sup>21</sup>Ludwig Boltzmann Institute for Rare and Undiagnosed Diseases, Vienna, Austria; <sup>22</sup>St. Anna Children's Cancer Research Institute, Vienna, Austria; <sup>23</sup>Pediatric Immunology and Infectious Disease, Bristol Royal Hospital for Children, Bristol, UK; <sup>24</sup>Specialized Immunology Laboratory of Dr. Shahrooei, Sina Medical Complex, Ahvaz, Iran; <sup>25</sup>Department of Microbiology and Immunology, Clinical and Diagnostic Immunology, Katholieke Universiteit Leuven, Leuven, Belgium; <sup>26</sup>Infection, Inflammation, and Rheumatology Section, Infection, Immunity, Inflammation and Physiological Medicine Programme, University College London Institute of Child Health, London, UK; <sup>27</sup>Department of Laboratory Medicine, Division of Clinical Immunology, Karolinska Institute at Karolinska University Hospital Huddinge, Stockholm, Sweden; <sup>28</sup>Research Center for Immunodeficiencies, Tehran University of Medical Sciences, Tehran, Iran; <sup>29</sup>Department of Pediatrics, Division of Allergy and Clinical Immunology, Tehran University of Medical Sciences, Tehran, Iran; <sup>30</sup>Research Center for Immunodeficiencies, Tehran University of Medical Sciences, Tehran, Iran; <sup>31</sup>Reference Center for Rare Rheumatic and Autoimmune Diseases in Children, Pediatric Rheumatology, Hospices Civils de Lyon, Centre International de Recherche en Infectiologie, Institut National de la Santé et de la Recherche Médicale U1111, UMS3444/US8 Lyon University, Lyon, France; <sup>32</sup>Howard Hughes Medical Institute, New York, NY; <sup>33</sup>Center for the Study of Primary Immunodeficiencies, Necker Hospital for Sick Children, Assistance Publique-Hôpitaux de Paris, Paris, France.

\*K. Moriya and A. Nieto-Patlán contributed equally to this paper; \*\*F. Dogu, S. Haskologlu, E. İnce, J. El-Benna, G. Uzel, A. Kiykim, K. Boztug, M.R. Roderick, M. Shahrooei, P.A. Brogan, H. Abolhassani, G. Hancioglu, N. Parvaneh, A. Belot, and A. Ikinciogullari contributed equally to this paper; \*\*\*J.-L. Casanova, A. Puel, and J. Bustamante contributed equally to this paper; Correspondence to Anna-Lena Neehus: [anna-lena.neehus@inserm.fr](mailto:anna-lena.neehus@inserm.fr); Jacinta Bustamante: [jacinta.bustamante@inserm.fr](mailto:jacinta.bustamante@inserm.fr); Anne Puel: [anne.puel@inserm.fr](mailto:anne.puel@inserm.fr); N. Lachmann's present address is Department for Pediatric Pneumology, Allergology and Neonatology, Hannover Medical School, RESIST Cluster of Excellence, Hannover, Germany.

© 2021 Neehus et al. This article is distributed under the terms of an Attribution-Noncommercial-Share Alike-No Mirror Sites license for the first six months after the publication date (see <http://www.rupress.org/terms/>). After six months it is available under a Creative Commons License (Attribution-Noncommercial-Share Alike 4.0 International license, as described at <https://creativecommons.org/licenses/by-nc-sa/4.0/>).

## Introduction

Protein kinase C  $\delta$  (PKC $\delta$ ) is a cytosolic kinase of the novel serine/threonine PKC group (diacylglycerol [DAG]-dependent, Ca<sup>2+</sup>-independent). It is ubiquitously expressed and is an essential regulator of immune homeostasis and B cell development in humans and mice (Guo et al., 2004; Griner and Kazanietz, 2007). It can be activated in response to various stimuli, leading to individual patterns of PKC $\delta$  phosphorylation and, thus, to the differential activation of various downstream targets. PKC $\delta$  is involved in regulating apoptosis, proliferation, and cell survival in various cells, including lymphocytes and phagocytes (Salzer et al., 2016; Reyland et al., 1999; Wu-Zhang et al., 2012; Gomel et al., 2007; DeVries-Seimon et al., 2007). It is activated by stimulation with DAG and phospholipids produced by the phospholipase C $\gamma$  (PLC $\gamma$ )-mediated hydrolysis of membrane inositol and phorbol esters (Nishizuka, 1995; Duquesnes et al., 2011). In addition to the conformational changes induced by binding to DAG, PKC $\delta$  requires autophosphorylation and phosphorylation by phosphoinositide-dependent kinase-1 (PDK-1) for activation (Durgan et al., 2007). Its enzymatic activity is modulated by members of the Src kinase family, protein tyrosine kinase 2 (PYK2), mechanistic target of rapamycin, and phosphoinositide 3-kinase (PI3K; Duquesnes et al., 2011; Li et al., 1994). PKC $\delta$  activity is regulated via its regulatory domain, which contains a pseudosubstrate domain and two conserved domains (C1 and C2-like), with hydrophobic residues within the C1 motif responsible for the binding of PKC $\delta$  to DAG and phorbol esters (e.g., PMA; Zhang et al., 1995; Kazanietz et al., 1995). The pseudosubstrate domain, which is located between the C1 and C2-like domains, blocks access to the substrate-binding pocket, keeping PKC $\delta$  in an inactive state. The enzymatic activity of PKC $\delta$  is dependent on the catalytic domain, composed of the C3 and C4 domains, containing the ATP- and substrate-binding sequences, respectively (Duquesnes et al., 2011; Pappa et al., 1998; Cho, 2001). Several proteins, including STAT1 and -3, nuclear factor of IL-6 (NF-IL6), and ERK1 and -2, have been identified as substrates of PKC $\delta$ , implicating this protein in diverse pathways (Salzer et al., 2016; Yang et al., 2019; Nishikawa et al., 1997).

Studies of *Prkcd* knockout mice have revealed an essential role for PKC $\delta$  in B cell homeostasis and tolerance, by demonstrating an accumulation of autoreactive B cells due to defective negative selection in germinal centers and autonomous B cell hyperproliferation (Mecklenbräuker et al., 2002; Limnander et al., 2011). *Prkcd*-knockout mice thus develop systemic autoimmunity, as shown by the presence of autoantibodies, immune complex-mediated glomerulonephritis, lymphadenopathy, and hepatosplenomegaly, with B cell infiltration in several organs and tissues (Mecklenbräuker et al., 2004; Miyamoto et al., 2002). Bone marrow neutrophils of PKC $\delta$  Y155F knock-in mice, lacking the key Y155 phosphorylation site and consequently displaying impaired translocation and activation of PKC $\delta$ , have low levels of ROS production and impaired neutrophil extracellular trap (NET) formation (Soroush et al., 2019; Humphries et al., 2008). PKC $\delta$ -deficient mice are highly susceptible to *Candida albicans* and *Aspergillus fumigatus*, probably due to impaired fungal killing by bone marrow neutrophils and impaired

ROS production, as shown for *C. albicans* (Li et al., 2016). PKC $\delta$  also plays a crucial role in the macrophage-mediated phagocytosis and clearance of *Listeria monocytogenes* and *Mycobacterium tuberculosis* via the production of ROS and reactive nitrogen species (Schwegmann et al., 2007). In murine and guinea pig neutrophils, PKC $\delta$  is required for the phosphorylation of p40<sup>phox</sup>, a subunit of the NADPH oxidase complex (Li et al., 2016; Someya et al., 1999). In particular, it mediates phosphorylation of the threonine 154 (T154) residue of p40<sup>phox</sup>, a key regulatory step in the activation of the NADPH oxidase complex in peripheral neutrophils and B cells, in both mice and humans (Chessa et al., 2010; Grandvaux et al., 2001; Belambri et al., 2018; Matute et al., 2005; Bouin et al., 1998). In human peripheral monocytes, peripheral B cells, and neutrophils, PKC $\delta$  mediates phosphorylation of the other phagocyte NADPH oxidase (phox) cytosolic subunits p67<sup>phox</sup>, p47<sup>phox</sup>, and p40<sup>phox</sup>, suggesting a more prominent regulatory function in ROS production (Grandvaux et al., 2001; Zhao et al., 2005; Bey et al., 2004; Brown et al., 2003).

Since 2013, 11 patients from 7 kindreds suffering from autosomal recessive (AR) PKC $\delta$  deficiency have been reported (Kuehn et al., 2013; Belot et al., 2013; Kiykim et al., 2015; Salzer et al., 2013; Lei et al., 2018; Nanthapaisal et al., 2017; Meyts et al., 2021; Sharifinejad et al., 2020). They manifested with a monogenic form of systemic lupus erythematosus (SLE) occurring before the age of 10 yr. These patients had small numbers of memory B cells (CD19<sup>+</sup>/CD27<sup>+</sup>), very large numbers of naive (CD19<sup>+</sup>/CD27<sup>-</sup>) and immature (CD19<sup>+</sup>/CD21<sup>-</sup>) B cells, and an impaired Ig class switch (Kuehn et al., 2013; Belot et al., 2013). High counts of circulating CD8<sup>+</sup> T cells and double-negative (CD4<sup>-</sup>/CD8<sup>-</sup>) T cells were observed in some cases, together with slightly low levels of T cell proliferation in vitro (Kuehn et al., 2013; Sharifinejad et al., 2020; Kiykim et al., 2015). Intriguingly, these patients suffer not only from autoimmune disease, but also from recurrent and/or severe infections (Kuehn et al., 2013; Belot et al., 2013; Kiykim et al., 2015; Salzer et al., 2013; Lei et al., 2018; Nanthapaisal et al., 2017; Meyts et al., 2021; Sharifinejad et al., 2020). In particular, PKC $\delta$ -deficient patients present viral, bacterial, and fungal infections, mostly affecting the lung, gastrointestinal tract, and lymph nodes, reminiscent of those seen in patients with chronic granulomatous disease (CGD). CGD is an inborn error of immunity caused by loss-of-function (LOF) or hypomorphic mutations of any of six genes encoding components of the NADPH oxidase complex (Thomas et al., 2019; Anjani et al., 2019). Like patients with CGD, PKC $\delta$ -deficient individuals have been reported to suffer from recurrent, and even invasive, bacterial infections, including in particular infections with *Staphylococcus* spp. and *Pseudomonas* spp. (Kuehn et al., 2013; Belot et al., 2013; Kiykim et al., 2015; Salzer et al., 2013; Lei et al., 2018; Nanthapaisal et al., 2017; Sharifinejad et al., 2020). The immunosuppressive treatment of SLE is a potential confounding factor, but we hypothesized that these patients might display an intrinsic susceptibility to infections. Based on the role of PKC $\delta$  in NADPH oxidase activation, and the overlap between the infections seen in patients with CGD and those with PKC $\delta$  deficiency, we tested the hypothesis that AR PKC $\delta$  deficiency impairs ROS production in phagocytic cells,

thereby underlying susceptibility to CGD-like infectious diseases. We therefore analyzed NADPH oxidase expression and activity in various subsets of myeloid cells, and in EBV-immortalized B cells (EBV-B cells) from all 11 previously reported patients and 6 newly identified patients with AR PKC $\delta$  deficiency.

## Results

### Clinical description of 17 patients with PKC $\delta$ deficiency

We studied 17 patients from 10 families originating from Mexico (kindred A), Turkey (kindreds B, D, H, and I), France (kindred C), Pakistan (kindred E), the UK (kindred F), and Iran (kindreds G and J; [Table 1](#) and [Fig. 1 A](#)). The 10 families were unrelated, and 6 were known to be consanguineous. 11 patients (P1–P10, P12) from 7 kindreds (A–G) have already been reported to have PKC $\delta$  deficiency ([Kuehn et al., 2013](#); [Belot et al., 2013](#); [Kiykim et al., 2015](#); [Salzer et al., 2013](#); [Lei et al., 2018](#); [Nanthapaisal et al., 2017](#); [Meyts et al., 2021](#); [Sharifinejad et al., 2020](#)). We identified five new patients by whole-exome sequencing (WES). The detailed clinical data of one patient (P11) will be reported elsewhere (unpublished data). Most patients (P1–P15) developed clinical manifestations before the age of 10 yr and displayed hepatosplenomegaly and various features of SLE, including photosensitivity, malar rash, alopecia, and oral ulcers, whereas P16 and P17 displayed no SLE-like symptoms. Furthermore, vasculitis and glomerulonephritis were documented in four (P1, P4, P7, and P8) and autoimmune hemolytic anemia in six (P1, P4, P7, P8, P14, and P15) patients. Most patients displayed B lymphoproliferation and/or high levels of autoreactive antinuclear antibodies (ANAs; P1–P15) or anti-double-stranded DNA (anti-dsDNA) antibodies, as found in nine patients (P3–P9, P12, and P13). In addition to SLE, the patients suffered from recurrent and/or severe infections ([Table 1](#)). All patients were vaccinated with *Bacillus Calmette-Guérin* (BCG) against tuberculosis, but only four patients (P13–P16) developed BCG-related disease. In addition, P13 also suffered from *Salmonella* bacteremia, recurrent gingivitis, and inguinal lymphadenitis due to *Staphylococcus aureus*. One patient suffered from severe *Legionella* pneumonia (P3); one from *Streptococcus pneumoniae* pneumonia (P12); one from *Listeria meningitis*, sepsis due to *Enterococcus faecium*, systemic *Candida* infection, and recurrent *Achromobacter xyloxidans* cervical lymphadenitis (P10); and one from sepsis caused by *Haemophilus influenzae* (P11). P4 died at the age of 13 yr, from septic shock due to *Pseudomonas aeruginosa* ([Table 1](#)). Five patients suffered from viral infections, most caused by herpesviruses, namely EBV (P1), CMV (P2), and varicella-zoster virus (P15), or other viruses, including papillomavirus (P3) and severe acute respiratory syndrome coronavirus 2 (SARS-CoV-2; P10). Six patients suffered from recurrent pneumonia (P1, P2, P3, P5, P6, and P12), four from recurrent otitis media (P1, P6, P10, and P12), and six from recurrent gastroenteritis (P2, P6, P11, P12, P14, and P15), although no causal microbe could be identified in any of these cases. Most patients were treated with corticosteroids (P1, P3–P9, and P12–P15), in combination with anti-CD20 antibodies in some cases (P4 and P6–P11), whereas one patient (P2) was successfully treated with hydroxychloroquine alone. Three

patients received mycophenolate mofetil (MMF; P4, P5, and P11), two received azathioprine (P7 and P8), and one was treated with sirolimus (P10). Most of the patients have received intravenous immunoglobulin (IVIG; P2, P5–P11, P13, and P15) and/or antibiotics (P2, P6, P12, and 13) as prophylaxis ([Table 1](#)).

### Biallelic PRKCD variants in 17 individuals from 10 families

Eight disease-causing *PRKCD* variants in 12 patients have been found: 10 patients (P1–P9 and P12) were found to be homozygous for rare *PRKCD* variants, including four missense variants (c.1840C>T [p.R614W], c.742G>A [p.G248S], c.1528G>A [p.G510S], and c.1294G>T [p.G432W]), one small insertion (c.1293\_1294insA, predicted p.G432Rfs\*15), and one essential splice site substitution (c.1352 + 1G>A; [Table 1](#) and [Fig. 1 A](#); [Kuehn et al., 2013](#); [Kiykim et al., 2015](#); [Belot et al., 2013](#); [Salzer et al., 2013](#); [Lei et al., 2018](#); [Nanthapaisal et al., 2017](#); [Sharifinejad et al., 2020](#)). Two patients, P10 and P11, were compound heterozygous for a nonsense variant (c.571C>T [p.Q191\*]) and a variant located at the essential splice acceptor site at the end of intron 9 (c.788-2A>G; [Meyts et al., 2021](#); unpublished data). The newly identified patients, P13–P17, were found to carry previously unknown homozygous *PRKCD* variants: P13 carried an essential splice site variant (c.571 + 2dup) located in intron 7, P14 and P15 carried a nonsense variant (c.1384C>T [p.Q462\*]), and P16 and P17 carried a small homozygous deletion of 1 bp (c.642del) predicted to lead to a premature stop codon (p.N214Kfs\*26; [Fig. 1, A and B](#); and [Table 1](#)). All variants, in all patients, were confirmed by Sanger sequencing, and when available, familial segregation analysis was performed, confirming that the disease followed an AR pattern of inheritance ([Fig. 1 A](#)). Surprisingly, one individual was homozygous for a variant but was asymptomatic at the age of 6 yr (kindred J, II.1, P17). 8 of the 11 variants had already been reported, but we completed the study in silico. 6 of the 11 variants studied were private and were absent from public databases (p.G432W, c.571 + 2dup, c.642del, c.788-2A>G, c.1293\_1294insA, and c.1352 + 1G>A), whereas 5 were reported in the heterozygous state in the Genome Aggregation Database (gnomAD v2.1.1; p.Q191\*, p.G248S, p.Q462\*, p.G510S, and p.R614W), with a minor allele frequency <10<sup>-4</sup> ([Fig. 1 C](#)). No homozygotes for any of these variants were found in public databases. All missense variants affected sites known to have been conserved over evolution and had combined annotation-dependent depletion (CADD) scores well above the mutation significance cutoff (MSC) of 26.5, whereas the variants predicted to affect splicing had a CADD score close to or slightly below the MSC ([Figs. 1 C and SI A](#)). Only six other non-synonymous variants of *PRKCD* were found in the homozygous state in the gnomAD database (v2.1.1) and our in-house cohort (Laboratory of Human Genetics of Infectious Diseases) of >9,500 patients with various infectious diseases. They were missense variants with CADD scores below the MSC and were, therefore, not predicted to be deleterious. These data strongly suggest that the 17 patients studied have AR PKC $\delta$  deficiency, consistent with previous reports ([Kuehn et al., 2013](#); [Belot et al., 2013](#); [Kiykim et al., 2015](#); [Salzer et al., 2013](#); [Lei et al., 2018](#); [Nanthapaisal et al., 2017](#); [Sharifinejad et al., 2020](#)).

### PRKCD splice site variants are predicted to encode truncated proteins

Essential splice site variants have been reported for *PRKCD*, but nothing is known about the consequences of these variants for

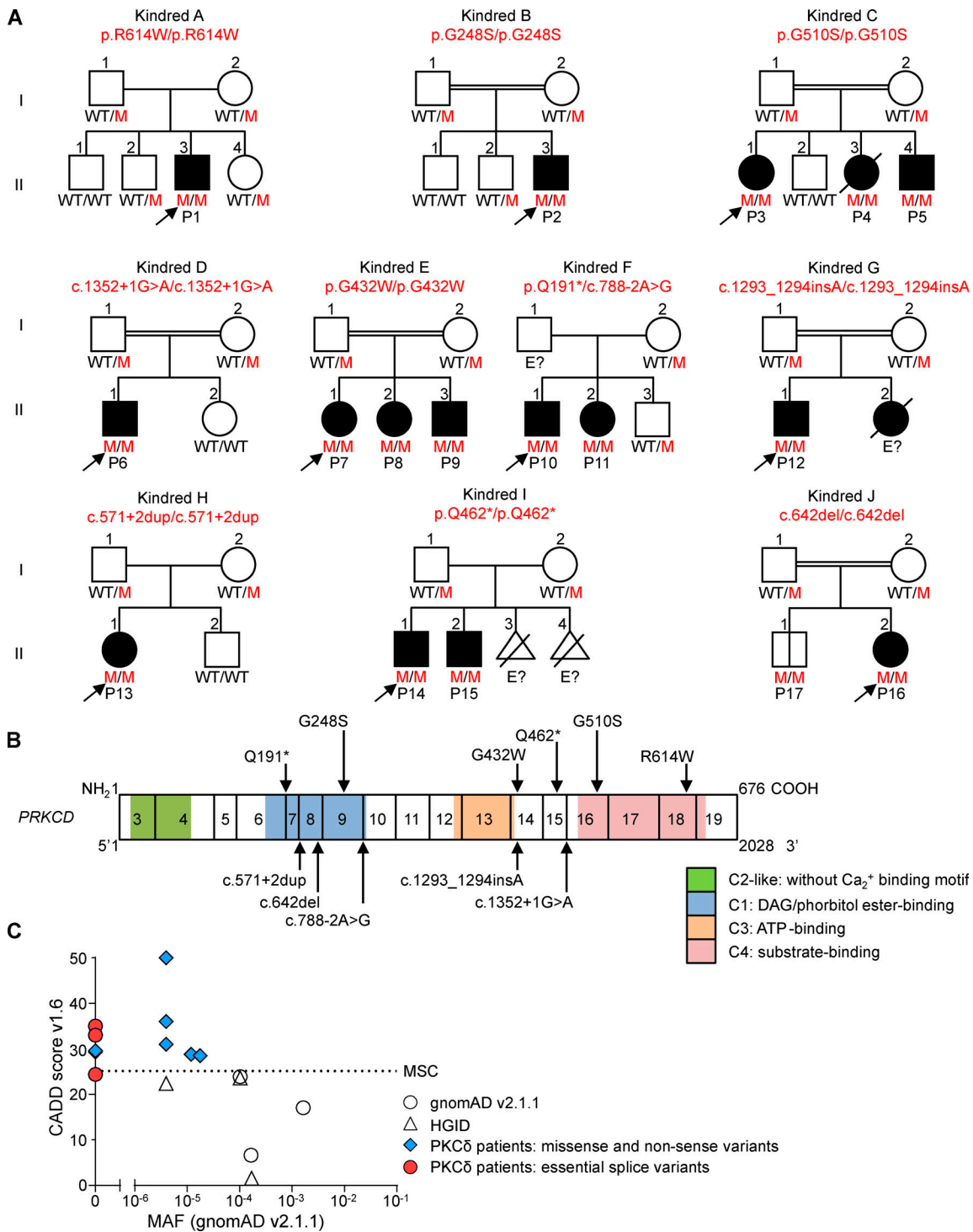
Table 1. The clinical spectrum of patients with PKC $\delta$  deficiency

Kindred	Patient	Mutation (predicted protein variant)	Origin	Sex	Follow-up	Age at onset of symptoms	Autoimmune manifestations	BCG status; clinical infectious phenotype (infections, microbiology, pathology results); treatment, prophylaxis	Reference
A	P1	c.1840C>T/c.1840C>T (p.R614W/p.R614W)	Mexico, living in USA	M	Alive	3 yr	Autoimmune hemolytic anemia, SLE ANA <sup>+</sup> , anti-RNP <sup>+</sup> , anti-smith <sup>+</sup> , anti-SSA <sup>+</sup>	BCG-vaccine: no AE; recurrent pneumonia, EBV infection, recurrent otitis media; corticosteroids, rapamycin; prophylaxis: NR	Kuehn et al., 2013
B	P2	c.742G>A/c.742G>A (p.G248S/p.G248S)	Turkey	M	Alive	1 yr	SLE ANA <sup>+</sup>	BCG-vaccine: no AE; recurrent pneumonia, CMV infection, recurrent gastroenteritis; hydroxychloroquine; prophylaxis: IVIG, antibiotics	Kiykim et al., 2015
C	P3	c.1528G>A/c.1528G>A (p.G510S/p.G510S)	France	F	Alive	10 yr	SLE ANA <sup>+</sup> , anti-dsDNA <sup>+</sup>	BCG-vaccine: no AE; severe Legionella pneumonia, recurrent pneumonia, severe papillomatosis; corticosteroids, hydroxychloroquine; prophylaxis: NR	Belot et al., 2013
	P4	c.1528G>A/c.1528G>A (p.G510S/p.G510S)		F	Dead	3 yr	Autoimmune hemolytic anemia, SLE ANA <sup>+</sup> , anti-dsDNA <sup>+</sup>	BCG-vaccine: no AE; died at age 13 yr from septic shock due to <i>P. aeruginosa</i> ; corticosteroids, MMF, anti-CD20 (rituximab); prophylaxis: NR	
	P5	c.1528G>A/c.1528G>A (p.G510S/p.G510S)		M	Alive	6 yr	SLE ANA <sup>+</sup> , anti-dsDNA <sup>+</sup>	BCG-vaccine: no AE; pleuritis and recurrent pneumonia; corticosteroids, MMF; prophylaxis: IVIG	
D	P6	c.1352+1G>A/c.1352+1G>A (??)	Turkey	M	Alive	1 yr	SLE ANA <sup>+</sup> , anti-dsDNA <sup>+</sup> , anti-cardiolipin <sup>+</sup>	BCG-vaccine: no AE; recurrent pneumonia, urinary tract infections, recurrent gastroenteritis, recurrent otitis media; corticosteroids, anti-CD20 (rituximab); prophylaxis: IVIG, antibiotics	Salzer et al., 2013
E	P7	c.1294G>T/c.1294G>T (p.G432W/p.G432W)	Pakistan, living in UK	F	Alive	1 yr	Autoimmune hemolytic anemia, SLE ANA <sup>+</sup> , anti-dsDNA <sup>+</sup>	BCG-vaccine: no AE; corticosteroids, anti-CD20 (rituximab), azathioprine; prophylaxis: IVIG	Lei et al., 2018; Nanthapaisal et al., 2017
	P8	c.1294G>T/c.1294G>T (p.G432W/p.G432W)		F	Alive	1 yr	Autoimmune hemolytic anemia, SLE ANA <sup>+</sup> , anti-dsDNA <sup>+</sup>	BCG-vaccine: no AE; cervical and inguinal lymphadenopathy; corticosteroids, anti-CD20 (rituximab), azathioprine; prophylaxis: IVIG	
	P9	c.1294G>T/c.1294G>T (p.G432W/p.G432W)		M	Alive	2 yr	SLE ANA <sup>+</sup> , anti-dsDNA <sup>+</sup>	BCG-vaccine: no AE; corticosteroids, anti-CD20 (ofatumumab); prophylaxis: IVIG	

Table 1. The clinical spectrum of patients with PKC $\delta$  deficiency (Continued)

Kindred	Patient	Mutation (predicted protein variant)	Origin	Sex	Follow-up	Age at onset of symptoms	Autoimmune manifestations	BCG status; clinical infectious phenotype (infections, microbiology, pathology results); treatment, prophylaxis	Reference
F	P10	c.788-2A>G/c.571C>T (p.Q191*)	UK	M	Alive	9 mo	SLE ANA <sup>+</sup>	BCG-vaccine: no AE; <i>Listeria meningitis</i> , recurrent otitis media, early-onset enterocolitis, systemic <i>Candida</i> infection, sepsis due to <i>E. faecium</i> , recurrent A. <i>xyloxidans</i> cervical lymphadenitis. SARS-CoV-2 infection; sirolimus, anti-CD20 (rituximab); prophylaxis: IVIG	Unpublished data; Meyts et al., 2021
	P11	c.788-2A>G/c.571C>T (p.Q191*)		F	Alive	6 mo	SLE ANA <sup>+</sup>	BCG-vaccine: no AE; <i>H. influenzae</i> sepsis, recurrent gastroenteritis, early-onset enterocolitis; MMF, anti-CD20 (rituximab); prophylaxis: IVIG	
G	P12	c.1293_1294insA/c.1293_1294insA (p.G432Rfs*15)/p.G432Rfs*15	Afghanistan, living in Iran	M	Alive	1 yr	SLE ANA <sup>+</sup> , anti-dsDNA <sup>+</sup>	BCG-vaccine: no AE; <i>S. pneumoniae</i> pneumonia, <i>H. influenzae</i> otitis media, recurrent oral candidiasis, recurrent pneumonia, recurrent gastroenteritis; corticosteroids, NSAIDs, azathioprine; prophylaxis: cyclic rotation of sulfamethoxazole-trimethoprim/amoxicillin and azithromycin	Sharifnejad et al., 2020
H	P13	c.571+2dup/c.571+2dup (??)	Turkey	F	Alive	1 yr	SLE ANA <sup>+</sup> , anti-dsDNA <sup>+</sup>	BCG-vaccine: at 2 mo of age, BCG-osis; <i>Salmonella</i> bacteremia; <i>S. aureus</i> inguinal lymphadenitis, recurrent gingivitis; antimycobacterial treatment, ceftriaxone; corticosteroids; prophylaxis: amoxicillin, IVIG	This paper
I	P14	c.1384C>T/c.1384C>T (p.Q462*)	Turkey	M	Alive	7 mo	Autoimmune hemolytic anemia, ANA <sup>+</sup>	BCG-vaccine: BCG-itis; recurrent gastroenteritis; isoniazid, rifampicin; corticosteroids; prophylaxis: none at present	This paper
	P15	c.1384C>T/c.1384C>T (p.Q462*)		M	Alive	7 mo	Autoimmune hemolytic anemia, ANA <sup>+</sup>	BCG vaccine: BCG-itis; recurrent gastroenteritis, shingles; isoniazid, rifampicin; corticosteroids; prophylaxis: IVIG	
J	P16	c.642del/c.642del (p.N214Kfs*26/p.N214Kfs*26)	Iran	F	Alive	1 yr	No SLE, ANA <sup>-</sup> , anti-dsDNA <sup>-</sup>	BCG vaccine: BCG-itis; isoniazid, rifampicin, azithromycin; prophylaxis: none at present	This paper
	P17	c.642del/c.642del (p.N214Kfs*26/p.N214Kfs*26)		M	Alive		No SLE, ANA <sup>-</sup> , anti-dsDNA <sup>-</sup>	BCG vaccine: no AE; asymptomatic; prophylaxis: none at present	

Family code, patient number, and mutations are as in Fig. 1. Predicted protein variations are indicated in parenthesis. ? indicates unknown prediction of splice site variants. Patient origin, sex, current vital status, age at onset of symptoms, and clinical phenotypes are shown. AE, adverse effect; F, female; M, male; NR, not reported; NSAID, nonsteroidal anti-inflammatory drug.



Downloaded from [http://rupress.org/jem/article-pdf/121/8/9620210501/1419330/jem\\_20210501.pdf](http://rupress.org/jem/article-pdf/121/8/9620210501/1419330/jem_20210501.pdf) by Uci Library Services user on 28 July 2021

**Figure 1. AR PKC $\delta$  deficiency in 10 families. (A)** Pedigree of the 10 unrelated kindreds showing familial segregation of the different *PRKCD* alleles. Generations are indicated by Roman numerals (I–II), and each individual is indicated by an Arabic numeral (1–4). Male and female individuals are represented by squares and circles, respectively. Double horizontal lines indicate consanguinity. Affected patients are represented by closed black symbols, the index cases are indicated by an arrow, and asymptomatic carriers are indicated by a black vertical line. Individuals of unknown genotype are indicated by “E?” Symbols crossed with a black diagonal line indicate deceased individuals. **(B)** Schematic representation of the *PRKCD* gene. Coding exons are numbered (3–19). The PKC $\delta$  protein is represented with four domains: C2-like, without Ca<sub>2</sub><sup>+</sup> binding motif; C1, binding to diacylglycerol and phorbol esters; C3, ATP-binding; and C4, substrate-binding domain. The positions of the variants observed in the patients are indicated by arrows. **(C)** Minor allele frequency (MAF) and CADD score for all *PRKCD* variants studied (colored symbols) or found in the homozygous state in gnomAD v2.1.1 (white circles; <https://gnomad.broadinstitute.org/>) or our in-house cohort (Laboratory of Human Genetics of Infectious Diseases [HGID]; white triangles). The missense and nonsense mutations of the patients are represented as blue lozenges, and essential splice site mutations are indicated by closed red circles. The dotted line corresponds to the MSC of 26.5, with its 95% confidence interval.

splicing (Salzer et al., 2013; Meyts et al., 2021). We assessed the impact of all the essential splice site variants identified, by performing topoisomerase-based cloning (TOPO-TA) on full-length cDNA and sequencing 100 transcripts for patients and controls (Fig. S1 B). We detected two aberrantly spliced variants for c.1352 + 1G>A (P6), leading to the skipping of exon 14 (22%; c.1261\_1352del; p.D421Vfs\*5) or to a 4-bp insertion between exons 14 and 15 (78%; c.1352\_1353ins4; p.F452Yfs\*6). For c.788-2A>G/p.Q191\* (P10 and P11), five transcripts were detected by TOPO-TA cloning: 52% of them corresponded to the p.Q191\* nonsense mutation, while 48% were aberrantly spliced, leading to a 38-bp deletion at the start of exon 10 (6%; c.788\_825del; p.D263Gfs\*14), the skipping of exon 10 (8%; c.788\_888del; p.D263Efs\*101), or the retention of 124 bp (16%; c.787\_788ins124; p.D263Efs\*9) or 140 bp (18%; c.787\_788ins140; p.D263Vfs\*34) of intron 9, respectively. Finally, the c.571 + 2dup (P13) allele encoded two aberrant transcripts, leading to the retention of 25 bp (45%; c.571\_572ins25; p.Q191Rfs\*1) or 29 bp (55%; c.571\_572ins29; p.Q191Rfs\*1) of intron 7, resulting in the same predicted truncated protein. Thus, all the detected transcripts were predicted to encode truncated proteins (Fig. S1 B). We also performed TOPO-TA cloning for the missense variant p.G248S (P2), as in silico analysis predicted the creation of a new splice acceptor site in exon 9. However, all the transcripts analyzed corresponded to the patient's variant, and no aberrantly spliced transcripts were detected. No WT transcripts were detected on analysis of the cDNA obtained from any of the patients. TOPO-TA cloning was not performed for the other variants, as in silico analysis predicted no impact on splicing, and no additional transcripts were detected after gel electrophoresis and full-length PCR.

### Seven of 11 PKC $\delta$ variants are complete LOF for autophosphorylation when overexpressed

There is strong evidence to suggest that all the reported *PRKCD* variants are disease causing, but few experimental data are available to decipher the impact of these variants in overexpression systems. We therefore studied the impact of the *PRKCD* variants by transiently transfecting human embryonic kidney (HEK)293T cells with C-terminally DDK-tagged WT (NM\_006254) or mutant *PRKCD* cDNAs encoding nonsense or missense mutations (p.Q191\*, p.G248S, p.G432W, p.Q462\*, p.G510S, and p.R614W), cDNAs encoding all *PRKCD* transcripts identified by TOPO-TA cloning or predicted to cause a frameshift (c.571\_572ins25, c.571\_572ins29, c.642del, c.787\_788ins124, c.787\_788ins140, c.788\_825del, c.788\_888del, c.1293\_1294insA, c.1261\_1352del, and c.1352\_1353ins4), and the cDNA for a previously described LOF mutant (c.1133A>T [p.K378M]), which served as negative control (Belot et al., 2013). All *PRKCD* mRNAs were produced in similar amounts, as shown by real-time quantitative PCR (RT-qPCR; Fig. 2 A). Protein expression and activity in the basal state were analyzed by Western blotting with antibodies against specific phosphorylation sites of PKC $\delta$  known to be required for protein activity (Fig. 2 B; Newton, 2001). The p.G248S, p.G432W, p.G510S, p.R614W, and p.K378M PKC $\delta$  variants were expressed at the same molecular weight as the WT protein, whereas transient transfection with cDNAs

encoding nonsense and frameshift *PRKCD* variants led to the expression of truncated proteins of lower molecular weight, consistent with in silico predictions (Figs. 2 B and S1 B). No reinitiation of translation downstream from the premature stop codons was observed, in analyses with an anti-DDK antibody (not depicted). All nonsense and frameshift variants were LOF for the autophosphorylation of PKC $\delta$  at the T505 and S643 residues, whereas p.G432W, p.G510S, and p.R614W were hypomorphic (Fig. 2, B and C). The p.G248S variant displayed no impairment of autophosphorylation. Taken together, these results indicate that the nonsense and frameshift mutations strongly impair PKC $\delta$  protein expression and abolish PKC $\delta$  autophosphorylation, and that all but one of the missense mutations strongly impair autophosphorylation, suggesting that these mutations are responsible for AR PKC $\delta$  deficiency.

### Altered PKC $\delta$ expression and function in the EBV-B cells of eight PKC $\delta$ -deficient patients

PKC $\delta$  is strongly expressed in human peripheral B lymphocytes and EBV-B cells (Mecklenbräuker et al., 2004; Kuehn et al., 2013; Salzer et al., 2013). We used EBV-B cells to assess the impact of the various mutations on mRNA and protein levels in an endogenous system. We evaluated *PRKCD* transcript levels in cells from patients and healthy controls by RT-qPCR, with two different probes spanning the junctions of exons 3 and 4 and of exons 17 and 18 (Fig. 3 A). No EBV-B cells were available for P4, P7–P9, P12, or P14–P17. Low levels of *PRKCD* transcripts were detected in EBV-B cells from P6, P10, P11, and P13; these transcripts carried nonsense or essential splice site mutations and were shown to encode truncated proteins (Figs. 3 A and S1 B). However, for P1–P3 and P5, *PRKCD* transcript levels were within the range of controls (Fig. 3 A). We further investigated PKC $\delta$  protein levels by Western blotting with whole-cell lysates. A total loss of PKC $\delta$  protein was observed in the EBV-B cells of P6, P10, P11, and P13 (Fig. 3 B). The essential splice site and nonsense mutations of these patients were predicted to result in truncated proteins, which were detected in overexpression experiments in HEK293T cells, but not in the patients' cells. However, low (P1, P3, and P5) or high (P2) PKC $\delta$  protein levels were detected in EBV-B cells carrying missense mutations (Fig. 3 B). We also assessed the functional consequences of PKC $\delta$  deficiency for autophosphorylation and PMA-induced apoptosis, as PKC $\delta$  is involved in proapoptotic signaling after phorbol ester stimulation or DNA damage (Fig. 3, C and D; Basu and Pal, 2010). Consistent with our previous overexpression findings, autophosphorylation was abolished (P1, P6, P10, P11, and P13) or impaired (P3 and P5) in the patients' EBV-B cells, except for those of P2, which displayed normal autophosphorylation (Fig. 3 C). However, the EBV-B cells of P2 displayed impaired myristoylated alanine-rich C-kinase substrate (MARCKS) phosphorylation in response to PMA stimulation (Fig. S2). The EBV-B cells of all the patients (including P2) were resistant to PMA-induced cell death but remained as sensitive as the EBV-B cells of healthy controls to alternative apoptosis inducers, such as FAS (Fig. 3 D; Kuehn et al., 2013). Overall, these findings suggest that *PRKCD* mRNAs carrying nonsense or frameshift mutations undergo nonsense-mediated mRNA decay, resulting in a loss of

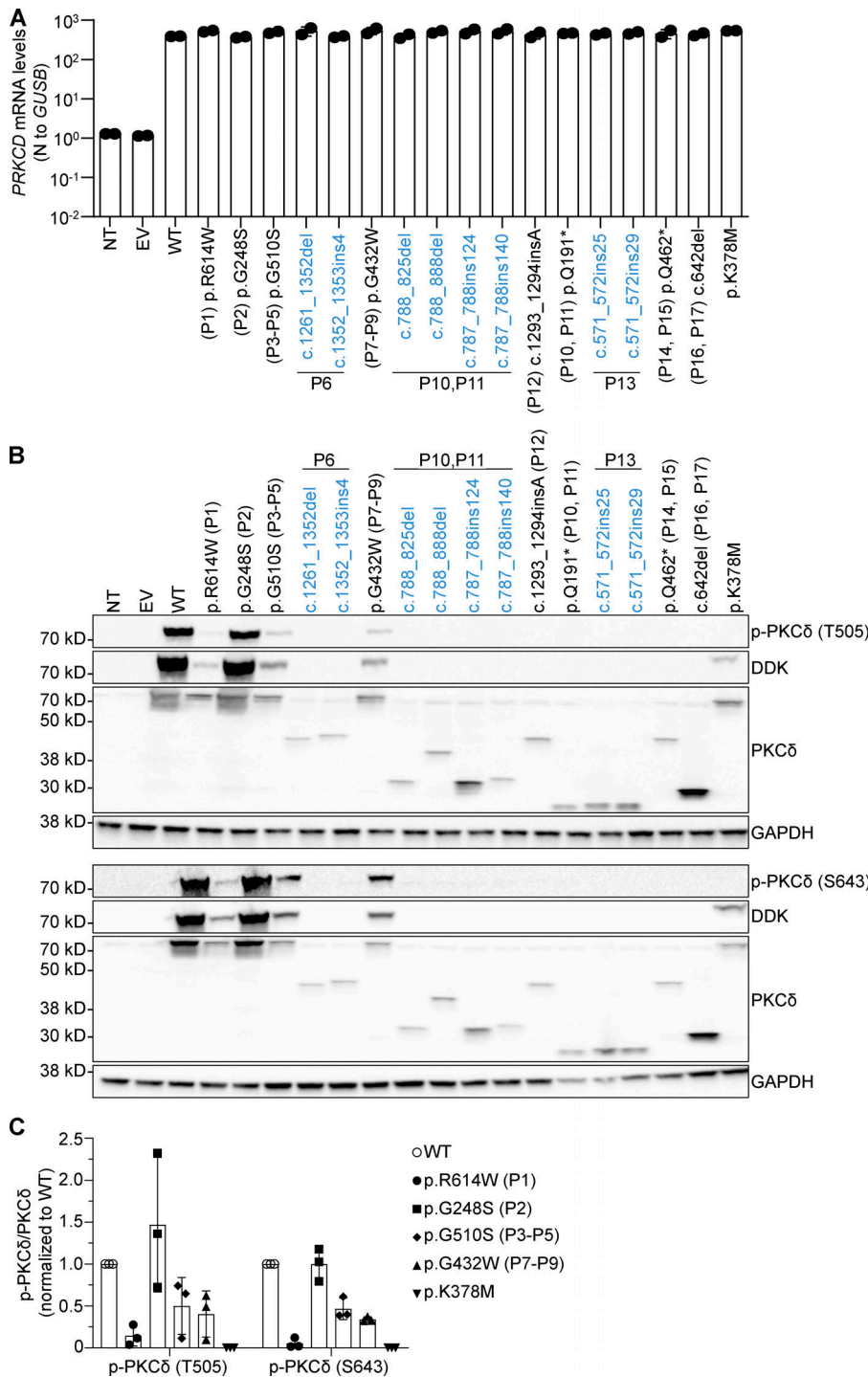


**Figure 2. In vitro characterization of the various PRKCD alleles in an overexpression system.** **(A)** RT-qPCR of cDNA from HEK293T cells non-transfected (NT) or transfected with an empty vector (EV), WT PRKCD, or mutated PRKCD. GUSB was used for normalization ( $n = 2$ ; mean  $\pm$  SD). **(B)** Western blot of total protein extracts from HEK293T cells either NT or transfected with EV, WT PRKCD, or mutated PRKCD, all inserted into pCMV6 with a C-terminal DDK tag. PKC $\delta$  was detected with a polyclonal anti-PKC $\delta$  antibody and an antibody directed against the C-terminal DDK tag. PKC $\delta$  phosphorylation was detected with polyclonal antibodies against the T505 (upper panel) and S643 (lower panel) phosphorylation sites. An antibody against GAPDH was used as a loading control. The results shown are representative of three independent experiments. Transcripts identified by TOPO-TA cloning are indicated in blue. **(C)** Quantification of phosphorylated PKC $\delta$  expression compared with the amount of total PKC $\delta$ . All values were normalized to the WT transfected cells ( $n = 3$ ; mean  $\pm$  SD).

Downloaded from [http://rupress.org/jem/article-pdf/118/9/2021/105011419330/jem\\_20210501.pdf](http://rupress.org/jem/article-pdf/118/9/2021/105011419330/jem_20210501.pdf) by Ucl Library Services user on 28 July 2021

expression of the PKC $\delta$  protein, whereas at least two of the missense mutations are associated with the production of smaller amounts of PKC $\delta$  protein. Strikingly, the EBV-B cells of all patients tested presented a defect of PMA-induced apoptosis, indicating a loss of PKC $\delta$  function.

**Impaired NADPH oxidase activity and complementation in the patients' EBV-B cells**

Members of the PKC family are known to be involved in NADPH oxidase activity in murine phagocytes, and PKC $\delta$ , in particular,

has been shown to regulate the activation of NADPH oxidase by phosphorylating p40<sup>phox</sup> (Li et al., 2016; Someya et al., 1999). However, the role of PKC $\delta$  in human phagocytes and EBV-B cells has been less studied (Li et al., 2016; Szilagyi et al., 2015). We therefore evaluated NADPH oxidase activity in EBV-B cells from patients with PKC $\delta$  deficiency, comparing the results with those for healthy controls, and cells from patients with CGD (X-linked recessive complete gp91<sup>phox</sup> deficiency and AR p40<sup>phox</sup> deficiency). The PMA-induced production of intracellular superoxide (O<sub>2</sub><sup>-</sup>), measured in a luminol chemiluminescence assay, was

strongly impaired in the EBV-B cells of all PKC $\delta$ -deficient patients tested relative to healthy controls, whereas the EBV-B cells of p40<sup>phox</sup>- and gp91<sup>phox</sup>-deficient patients had impaired and abolished O<sub>2</sub><sup>-</sup> production, respectively (Fig. 4 A, left). Similarly, a strong decrease in O<sub>2</sub><sup>-</sup> production by EBV-B cells was observed for all PKC $\delta$ -deficient patients tested following stimulation with heat-killed *S. aureus* cells (Pansorbin), for receptor-mediated NADPH oxidase activation (Fig. 4 A, right). In addition, analyses of Amplex Red oxidation after PMA stimulation showed that much less hydrogen peroxide (H<sub>2</sub>O<sub>2</sub>) was released by the EBV-B cells of all PKC $\delta$ -deficient patients tested than by the EBV-B cells of healthy controls, with the amount of H<sub>2</sub>O<sub>2</sub> released by the patients' cells being similar to that released by EBV-B cells from patients with p40<sup>phox</sup> deficiency (Fig. 4 B). H<sub>2</sub>O<sub>2</sub> production in response to PMA was restored in the EBV-B cells of all patients by retroviral transduction with the WT *PRKCD* cDNA, as shown by Amplex Red oxidation (Figs. 4 C and S3). We also evaluated the impact of all the *PRKCD* alleles identified on ROS production by EBV-B cells, by transducing EBV-B cells from P13 (*PRKCD*<sup>-/-</sup>) with WT and all mutant-*PRKCD* cDNAs. In *PRKCD*<sup>-/-</sup> EBV-B cells, H<sub>2</sub>O<sub>2</sub> production was restored only by the overexpression of the *PRKCD* WT allele. H<sub>2</sub>O<sub>2</sub> production was not increased by transduction with any of the mutant alleles (Fig. 4 D). These findings demonstrate that PKC $\delta$  plays a nonredundant role in the activation of the NADPH oxidase in EBV-B cells.

#### Interaction of PKC $\delta$ with p40<sup>phox</sup>/p47<sup>phox</sup> and impaired p40<sup>phox</sup> phosphorylation in the patients' EBV-B cells

We investigated the mechanism underlying the impaired NADPH oxidase activity, by first evaluating the expression of all known NADPH oxidase subunits in the patients' EBV-B cells. Western blotting showed that all subunits of the NADPH oxidase (gp91<sup>phox</sup>, p67<sup>phox</sup>, p47<sup>phox</sup>, p40<sup>phox</sup>, p22<sup>phox</sup>, and EROS) were produced in normal amounts in EBV-B cells from all the PKC $\delta$ -deficient patients studied (Fig. 5 A). Flow cytometry confirmed the normal levels of gp91<sup>phox</sup>, p67<sup>phox</sup>, p47<sup>phox</sup>, p22<sup>phox</sup>, and cytochrome b<sub>558</sub>, the membrane complex formed by gp91<sup>phox</sup> and p22<sup>phox</sup> (Fig. S4 A). We then investigated possible interactions between PKC $\delta$  and all known subunits of the NADPH oxidase, by performing coimmunoprecipitation experiments in an overexpression system based on HEK293T cells. Immunoprecipitation and immunoblotting confirmed an interaction between p40<sup>phox</sup> and PKC $\delta$  and between p47<sup>phox</sup> and PKC $\delta$  (Fig. 5 B and Fig. S4, B and C). However, PKC $\delta$  did not interact with the other cytosolic (p67<sup>phox</sup> and RAC2) or membrane-bound (gp91<sup>phox</sup>, p22<sup>phox</sup>, and EROS) subunits (Fig. 5, C-E; and Fig. S4, D and E). Overexpression of PKC $\delta$  with p40<sup>phox</sup> or p47<sup>phox</sup> in HEK293T cells showed that PKC $\delta$  was able to phosphorylate both proteins when coexpressed (Fig. 5, F and G). Interestingly, the level of p40<sup>phox</sup> phosphorylation at the T154 residue was much lower in the EBV-B cells of the PKC $\delta$ -deficient patients than in those of the controls after PMA and *S. aureus* stimulation, whereas the phosphorylation of p47<sup>phox</sup> at two known PKC $\delta$  target residues (S304 and S315) remained similar to that in control EBV-B cells (Fig. 6, A-D; Fontayne et al., 2002). Phosphorylation at other known PKC $\delta$ -target sites of p47<sup>phox</sup> (S320, S328, and S379) could not be evaluated due to a lack of specific antibodies. The transduction of EBV-B cells

with *PRKCD* WT cDNA restored p40<sup>phox</sup> phosphorylation, for all the patients studied (Fig. 6 E). In conclusion, the EBV-B cells of patients with PKC $\delta$  deficiency have impaired ROS production, associated with lower levels of phosphorylation of the cytosolic NADPH oxidase subunit p40<sup>phox</sup> by PKC $\delta$ .

#### Impact of PKC $\delta$ deficiency on NADPH oxidase activity in the patients' phagocytic cells

Because the EBV-B cells of PKC $\delta$ -deficient patients had very low levels of ROS production, we investigated NADPH oxidase activity in response to various stimuli in the primary cells of the patients. In particular, we assessed dihydrorhodamine 123 (DHR) oxidation, which detects intracellular H<sub>2</sub>O<sub>2</sub> production, in neutrophils and monocytes following stimulation with PMA or serum-opsonized *Escherichia coli*. The patients' neutrophils and monocytes displayed impaired but not abolished DHR oxidation in response to both stimuli, like the cells of patients with inherited p40<sup>phox</sup> deficiency (Fig. 7, A and B; and Fig. S5, A and B). In addition, neutrophils and monocytes of P3 and P13 showed low or abolished PKC $\delta$  expression, respectively (Fig. S5 C). We also evaluated the formation of NETs by neutrophils from three patients (P3, P16, and P17) from two unrelated kindreds following stimulation with PMA. NET formation was strongly impaired in the patients' cells, whereas it was abolished in cells from a gp91<sup>phox</sup>-deficient patient (Figs. 7 C and S5 D). We also explored NADPH oxidase activity in monocyte-derived macrophages (MDMs). MDMs from all the patients tested displayed impaired H<sub>2</sub>O<sub>2</sub> release following stimulation with IFN- $\gamma$ , IFN- $\gamma$  plus PMA, or PMA alone, relative to healthy controls or patients with p40<sup>phox</sup> deficiency (Figs. 7 D and S5 E). Similarly, the NADPH oxidase activity of monocyte-derived dendritic cells (MDDCs), evaluated by assessing H<sub>2</sub>O<sub>2</sub> release after stimulation with LPS, LPS plus PMA, or PMA, was weaker than that of cells from healthy controls and p40<sup>phox</sup>-deficient patients (Fig. 7 E). As observed for EBV-B cells, the patients' MDMs displayed reduced or abolished PKC $\delta$  expression as well as impaired p40<sup>phox</sup> phosphorylation at the T154 residue, but normal p47<sup>phox</sup> phosphorylation at two other residues (S304 and S315) tested (Figs. 7 F and S5 F). The primary phagocytes of heterozygous relatives of PKC $\delta$ -deficient patients displayed no defects of ROS production (not depicted). Overall, these data suggest that PKC $\delta$  is essential for NADPH oxidase activation and NET formation in primary phagocytic cells, possibly through the phosphorylation of p40<sup>phox</sup>.

#### Discussion

We report an impairment of NADPH oxidase activity in 17 patients from 10 unrelated families with AR PKC $\delta$  deficiency. ROS production was severely impaired in the EBV-B cells, primary phagocytes (neutrophils and monocytes), MDMs, and MDDCs of all patients studied (Table 2). The transduction of the patients' EBV-B cells with WT *PRKCD* cDNA restored not only ROS production, but also the phosphorylation of p40<sup>phox</sup> on the T154 residue after PMA stimulation, strongly suggesting a role for PKC $\delta$  in activation of the NADPH oxidase complex. The

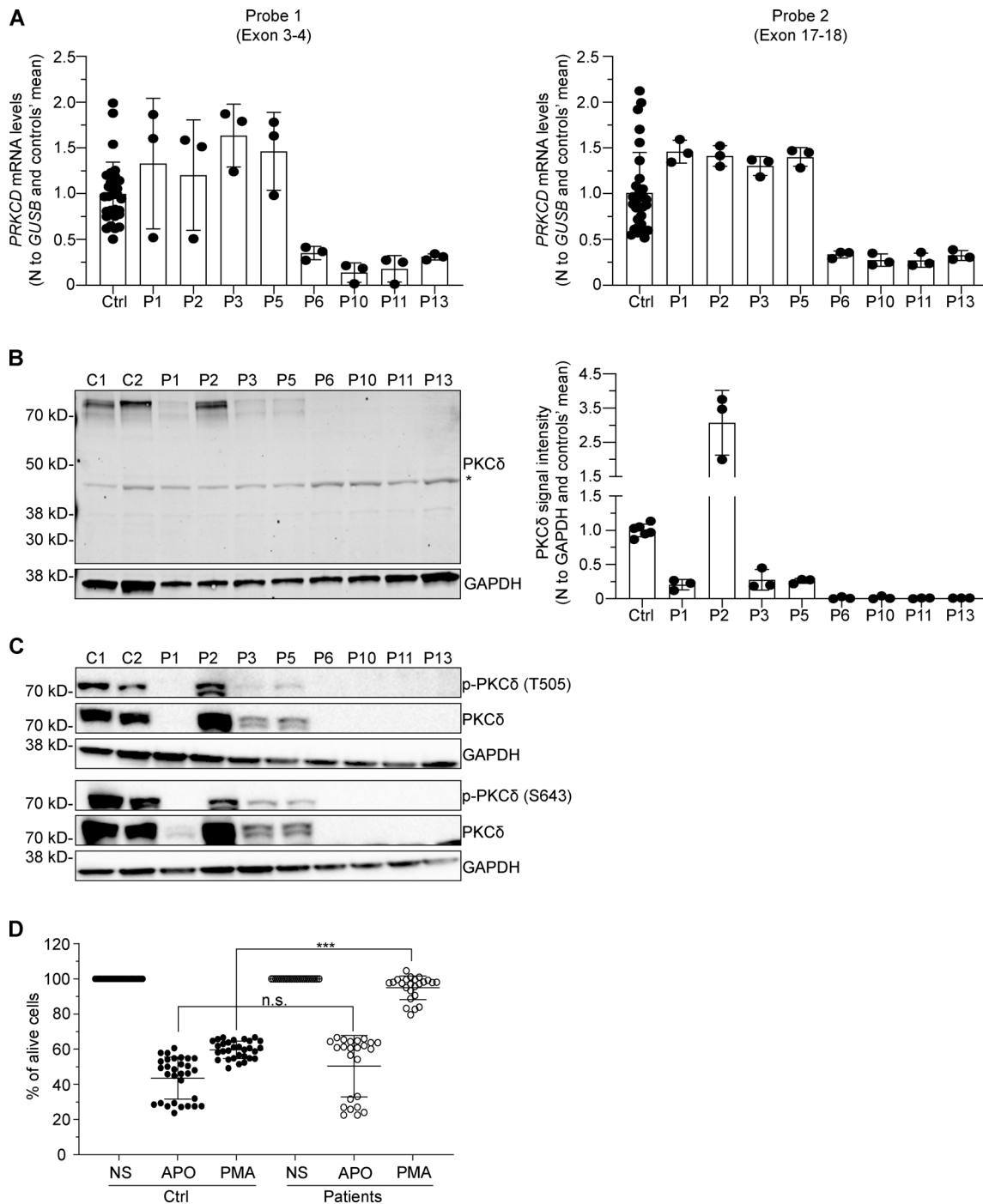
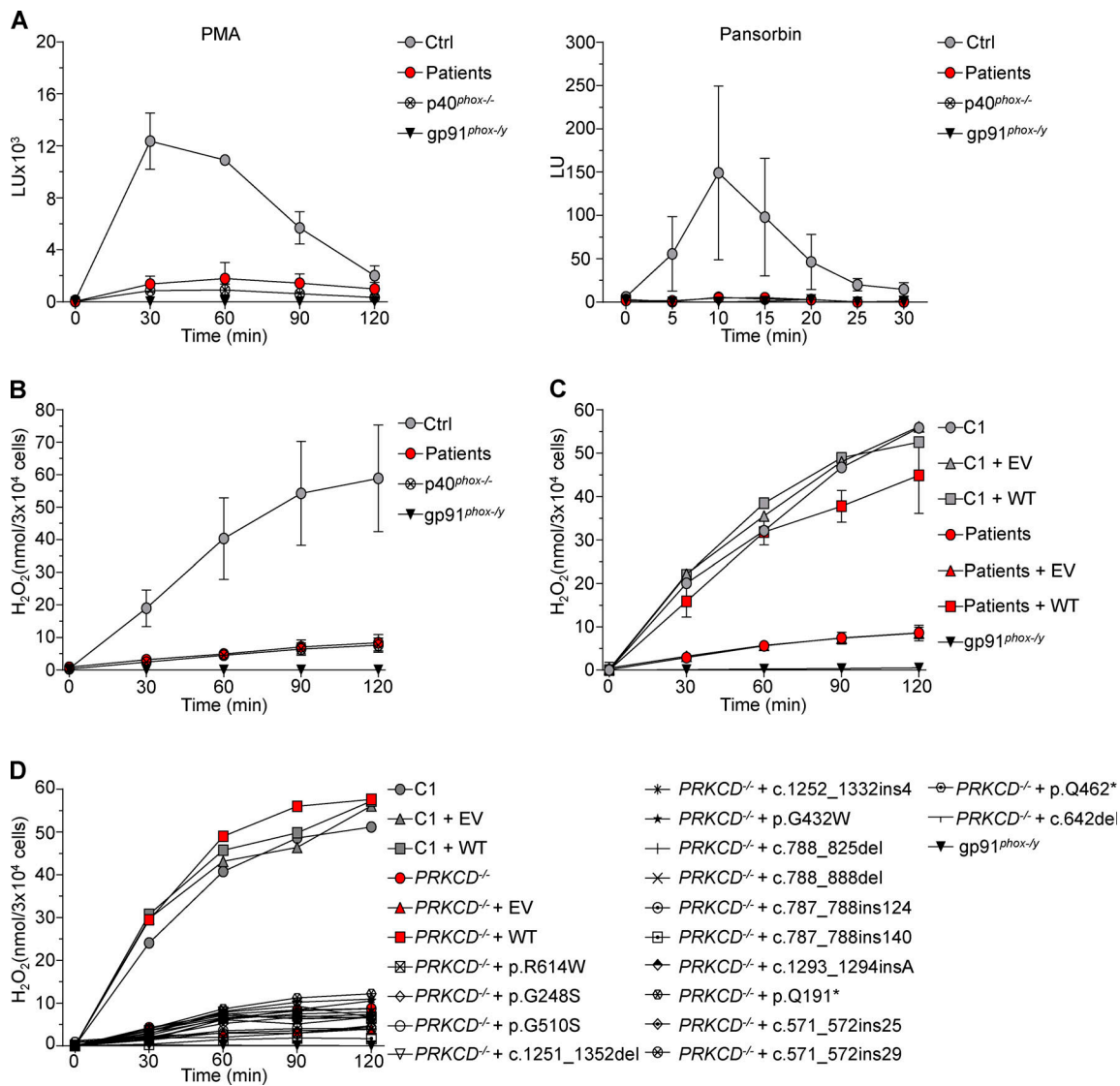


Figure 3. **PKC $\delta$  deficiency in patients' EBV-B cells.** (A) RT-qPCR for *PRKCD* with a probe spanning the junction between exons 3 and 4 (left) and a probe spanning the junction between exons 17 and 18 (right), in EBV-B cells from healthy controls (Ctrl;  $n = 10$ ) and patients. *GUSB* was used for normalization ( $n = 3$ ; mean  $\pm$  SD). (B) Western blot of total protein extracts from EBV-B cells from healthy controls (C1, C2) and patients (left). PKC $\delta$  was detected with a polyclonal anti-PKC $\delta$  antibody. The asterisk indicates nonspecific bands. Quantification of the PKC $\delta$  protein normalized against GAPDH (right;  $n = 3$ ; mean  $\pm$  SD). The results shown are representative of three independent experiments. (C) Western blot of total protein extract from the EBV-B cells of controls or patients. PKC $\delta$  was detected with a polyclonal anti-PKC $\delta$  antibody. The autophosphorylation of PKC $\delta$  was detected with antibodies against the T505 (upper panel) and S643 (lower panel) phosphorylation sites. The results shown are representative of three independent experiments. (D) Apoptosis of EBV-B cells from healthy controls (Ctrl;  $n = 10$ ) and patients ( $n = 8$ ) after 24 h of stimulation with APO-1-1 (APO; 1  $\mu$ g/ml) or PMA (100 ng/ml). The percentages of live cells were normalized against the number of nonstimulated (NS) cells, after acquisition by flow cytometry over a constant time ( $n = 3$ ; mean  $\pm$  SD). A linear mixed model was used to determine whether survival rates were the same for PKC $\delta$ -deficient patients and controls after APO or PMA stimulation (n.s., not significant; \*\*\*,  $P < 0.001$ ).



**Figure 4. NADPH oxidase activity and retroviral transduction of the patients' EBV-B cells. (A)** Production of  $O_2^-$  by EBV-B cells from healthy controls (Ctrl;  $n = 3$ ), PKC $\delta$ -deficient patients ( $n = 8$ ), p40<sup>phox</sup>-deficient patients ( $n = 2$ ), and gp91<sup>phox</sup>-deficient patients ( $n = 1$ ) after stimulation with PMA stimulation (left; 400 ng/ml) or Pansorbin (right; 2 mg/ml), as assessed by luminol bioluminescence. LU, luminescence units. The results shown are representative of two or three independent experiments. **(B)** Extracellular  $H_2O_2$  production by EBV-B cells from healthy controls ( $n = 3$ ), PKC $\delta$ -deficient patients ( $n = 8$ ), p40<sup>phox</sup>-deficient patients ( $n = 2$ ), and gp91<sup>phox</sup>-deficient patients ( $n = 1$ ) after PMA stimulation (400 ng/ml), as assessed with the Amplex Red test. The results shown are representative of three independent experiments. **(C)** Extracellular  $H_2O_2$  production by EBV-B cells from a healthy control (C1), a gp91<sup>phox</sup>-deficient patient, and PKC $\delta$ -deficient patients ( $n = 8$ ) transduced with an empty vector (EV) or PRKCD WT cDNA, after PMA stimulation (400 ng/ml), as assessed with the Amplex Red test (mean  $\pm$  SD). The results shown are representative of two independent experiments. **(D)** Production of  $H_2O_2$  by healthy control (C1), and PRKCD<sup>-/-</sup> EBV-B cells transduced with EV, WT, or the various mutant PRKCD cDNAs, upon PMA stimulation (400 ng/ml), as assessed with the Amplex Red test. The results shown are representative of two independent experiments.

phosphorylation of the T154 residue of p40<sup>phox</sup> is a key regulatory step in neutrophils and B lymphocytes, leading to assembly of the soluble cytosolic NADPH oxidase subunits with the membrane cytochrome *b*<sub>558</sub> (Someya et al., 1999; Chessa et al., 2010; Grandvaux et al., 2001; van de Geer et al., 2018; Matute et al., 2005). Indeed, the MDMs of the PKC $\delta$ -deficient patients displayed impaired p40<sup>phox</sup> phosphorylation and very low levels of ROS production. However, the MDMs of p40<sup>phox</sup>-deficient patients displayed normal ROS production, indicating that these cells are not dependent on p40<sup>phox</sup>, and therefore on p40<sup>phox</sup> phosphorylation, for PMA-induced ROS production.

These findings suggest the requirement of another PKC $\delta$  substrate for normal ROS production.

Coexpression and coimmunoprecipitation experiments showed that PKC $\delta$  interacted not only with p40<sup>phox</sup>, but also with p47<sup>phox</sup>, and was able to phosphorylate both proteins. Like p40<sup>phox</sup>, p47<sup>phox</sup> must undergo phosphorylation at various residues for translocation and binding to p22<sup>phox</sup> (El-Benna et al., 2009). Interestingly, we detected no abnormal phosphorylation of p47<sup>phox</sup> on the S304 and S315 residues in EBV-B cells or MDMs from PKC $\delta$ -deficient patients. As several PKC isoforms have been reported to mediate p47<sup>phox</sup> phosphorylation in human

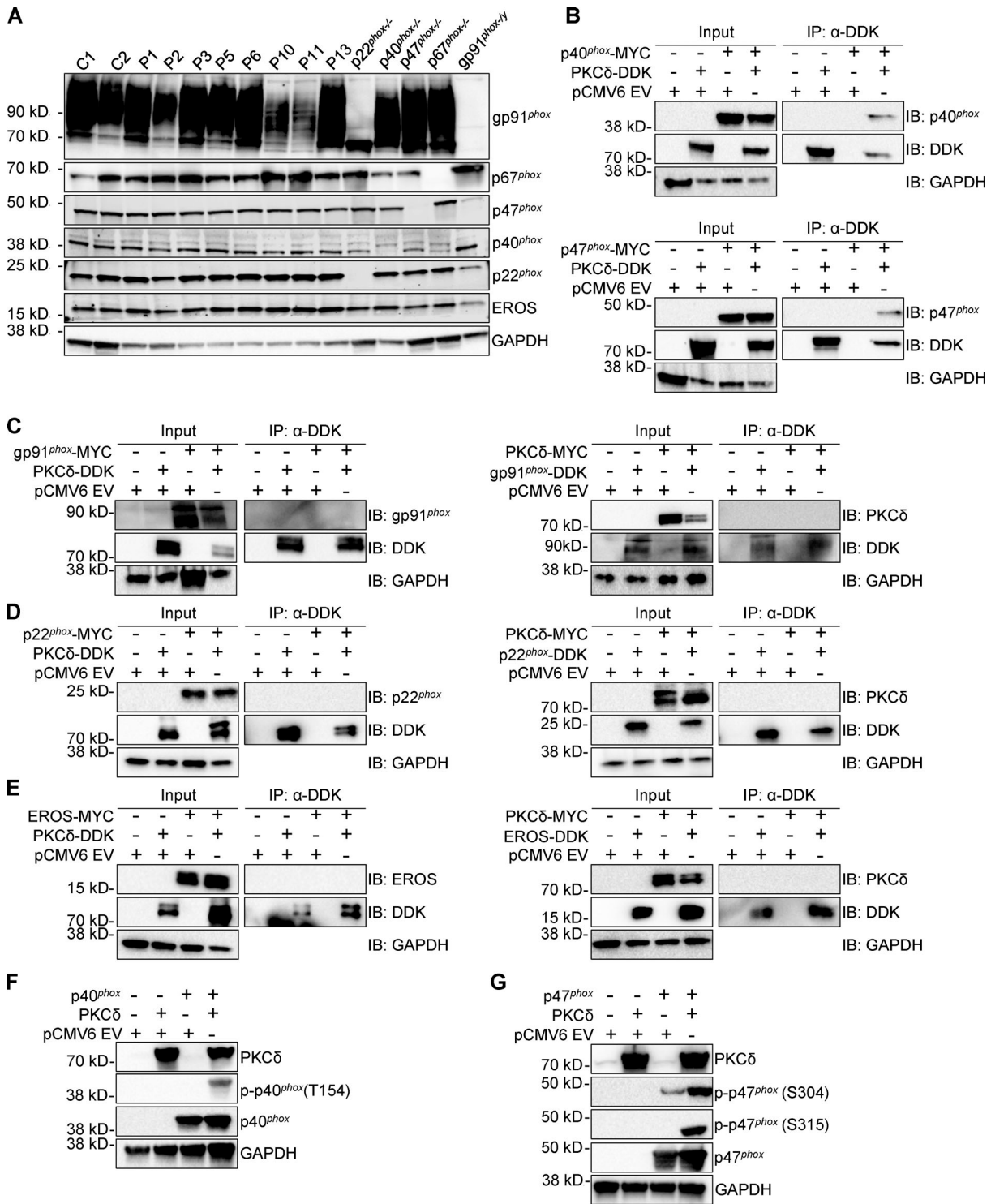


Figure 5. **NADPH oxidase subunit expression and interaction with PKCδ.** (A) Western blot of total protein extracts from the EBV-B cells of healthy controls (C1, C2), PKCδ-deficient patients and CGD patients. Antibodies against gp91<sup>phox</sup>, p67<sup>phox</sup>, p47<sup>phox</sup>, p40<sup>phox</sup>, p22<sup>phox</sup>, and EROS were used. An antibody against GAPDH was used as a loading control. (B) Coimmunoprecipitation (IP) of protein lysates from HEK293T cells transfected with empty vector (EV) or plasmids encoding PKCδ, p40<sup>phox</sup>, or p47<sup>phox</sup>. Pulldowns with anti-DDK (PKCδ) and immunoblots (IB) with anti-DDK or specific antibodies (p40<sup>phox</sup>, upper panel; p47<sup>phox</sup>, lower panel) are shown. (C) IP on protein lysates from HEK293T cells transfected with EV, CYBB, or PRKCD cDNAs. The pulldown of PKCδ (left) and gp91<sup>phox</sup> (right) was performed with an anti-DDK antibody. (D) IP on protein lysates from HEK293T cells transfected with the EV, CYBA, or PRKCD cDNAs. The pulldown of PKCδ (left) and p22<sup>phox</sup> (right) was performed with an anti-DDK antibody. (E) IP on protein lysates from HEK293T cells transfected with EV, CYBB, or PRKCD cDNAs. The pulldown of PKCδ (left) and EROS (right) was performed with an anti-DDK antibody. (F and G) Detection of p40<sup>phox</sup> (F) and p47<sup>phox</sup> (G) phosphorylation by Western blot on cell lysates of HEK293T cells transfected with EV, NCF4, NCF1, and PRKCD cDNAs. Representative images of three independent experiments.

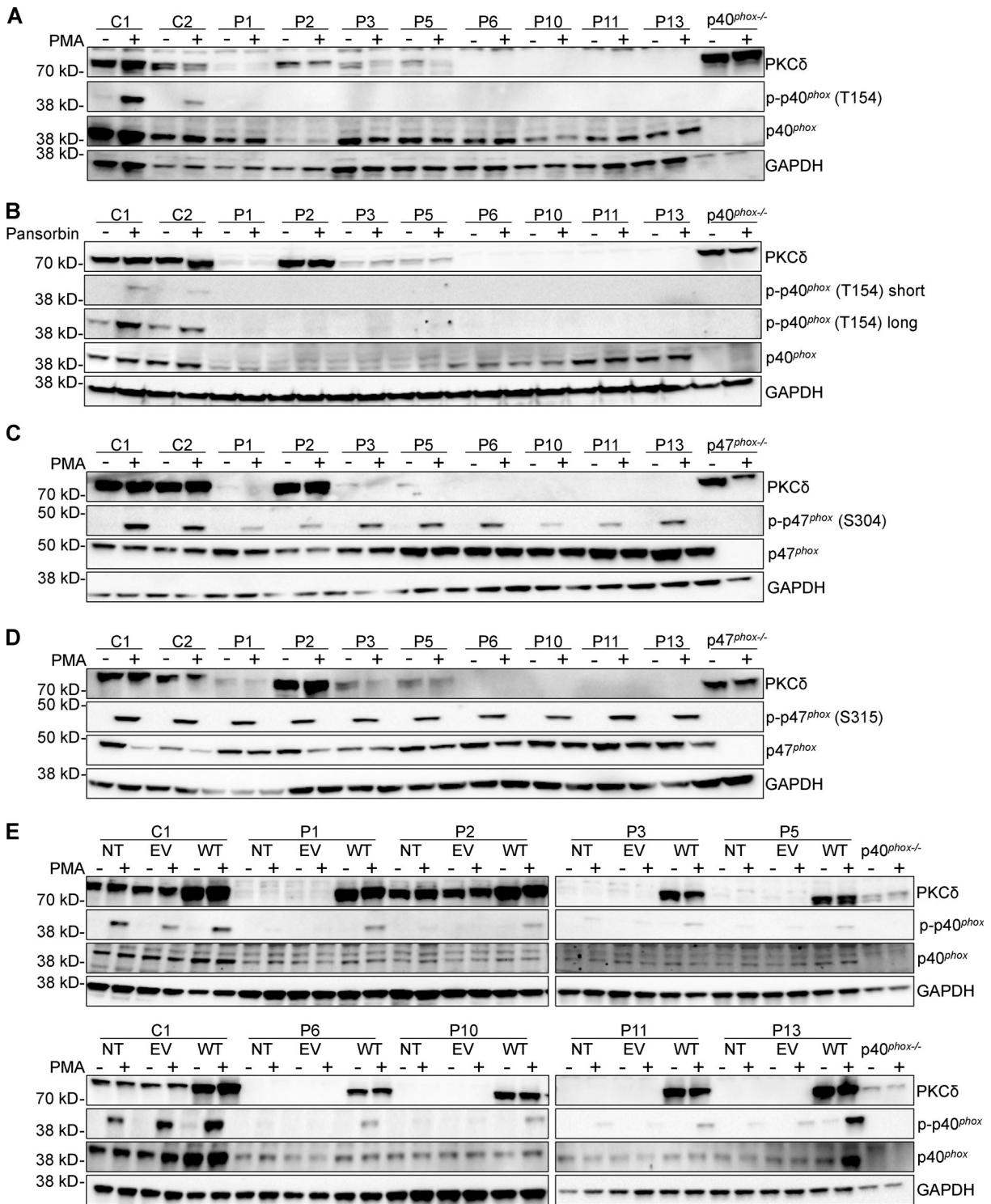


Figure 6. **p40<sup>phox</sup> and p47<sup>phox</sup> phosphorylation in PKCδ-deficient EBV-B cells.** (A) Phosphorylation of p40<sup>phox</sup> in total protein extracts from EBV-B cells of healthy controls (C1, C2), PKCδ-deficient patients, and a p40<sup>phox</sup>-deficient patient, before (-) and after (+) 30 min of PMA stimulation (400 ng/ml), measured by Western blot. (B) Phosphorylation of p40<sup>phox</sup> in total protein extracts from EBV-B cells of healthy controls, PKCδ-deficient patients, and a p40<sup>phox</sup>-deficient patient, before (-) and after (+) 30 min of Pansorbin stimulation (2 mg/ml), measured by Western blot. (C) Phosphorylation of p47<sup>phox</sup> in EBV-B cells of healthy controls, PKCδ-deficient patients, and a p47<sup>phox</sup>-deficient patient before (-) and after (+) 30 min of PMA stimulation (400 ng/ml), measured by Western blot. (D) Phosphorylation of p47<sup>phox</sup> in total protein extracts from the EBV-B cells of healthy controls, PKCδ-deficient patients, and a p47<sup>phox</sup>-deficient patient, before (-) and after (+) 30 min of PMA stimulation (400 ng/ml), measured by Western blot. (E) Phosphorylation of p40<sup>phox</sup> in total protein extracts from EBV-B cells of a healthy control, and PKCδ-deficient patients either nontransduced (NT) or transduced with an EV or PRKCD WT cDNA, before (-) and after (+) 30 min of PMA stimulation (400 ng/ml). Total protein extracts from EBV-B cells of a p40<sup>phox</sup>-deficient patient were used as controls. All results shown are representative of two to three independent experiments.

neutrophils, this suggests that PKC $\delta$  is redundant for p47<sup>phox</sup> phosphorylation at these residues (Bey et al., 2004; Fontayne et al., 2002; Segal et al., 2000). However, p47<sup>phox</sup> phosphorylation at S379 appears to be the most relevant for its activation and was shown to be a PKC $\delta$  target site (Fontayne et al., 2002; Meijles et al., 2014). Unfortunately, no antibodies are yet available for the evaluation of p47<sup>phox</sup> phosphorylation at S379, and further studies are required to evaluate the exact contribution of PKC $\delta$  to p47<sup>phox</sup> phosphorylation at various sites.

In all subsets of primary (neutrophils and monocytes) or monocyte-derived (MDMs and MDDCs) phagocytic cells tested after stimulation with PMA or *E. coli*, we observed no difference in ROS production or p40<sup>phox</sup> phosphorylation between patients with and without corticosteroid treatment. In addition to the low level of ROS production in neutrophils and monocytes after stimulation with PMA or *E. coli*, we observed a strong impairment of NET formation in PKC $\delta$ -deficient neutrophils, potentially contributing further to the impairment of bactericidal and fungicidal activity. In addition, a previous study reported a neutrophil killing defect in response to *E. coli* and *C. albicans* in PKC $\delta$ -deficient neutrophils from three of our patients (P3, P5, and P6; Szilagyi et al., 2015). These data are consistent with those obtained for Pkc $\delta$ -deficient mice, which display poor ROS production by bone marrow neutrophils, impaired NET formation, and impaired killing of *C. albicans* (Sorouh et al., 2019; Li et al., 2016). Further studies are required to determine the contributions of PKC $\delta$  to the assembly and activity of the NADPH oxidase and pathogen killing. In this respect, patient-derived induced pluripotent stem cells could be used to generate various subsets of myeloid cells. A humanized mouse model could also be used to dissect the development of different subsets of phagocytic cells and their contribution to ROS production (Neehus et al., 2018; Sontag et al., 2017; Lachmann et al., 2015; Evren et al., 2020). Overall, our data suggest that PKC $\delta$  is important for host innate immunity through its role in NADPH oxidase activation.

Our studies of NADPH oxidase activity in PKC $\delta$ -deficient cells revealed a cellular phenotype related to, but different from, that seen in patients with classic CGD, more closely resembling that seen in patients with p40<sup>phox</sup> deficiency (van de Geer et al., 2018; Wright et al., 2019; Matute et al., 2009). The defect of ROS production in PKC $\delta$ -deficient patients probably at least partly accounts for the recurrent and/or severe infections observed in these patients. The patients studied had recurrent bacterial infections, mostly affecting the lungs, lymph nodes, and gastrointestinal tract (Kuehn et al., 2013; Belot et al., 2013; Kiykim et al., 2015; Salzer et al., 2013; Lei et al., 2018; Nanthapaisal et al., 2017; Meyts et al., 2021; Sharifinejad et al., 2020; unpublished data). Two patients had invasive infections, one (P10, who survived infection) with *Candida* and another (P4, who died) with *P. aeruginosa*. Recurrent pneumonia and infections with *S. aureus* are also frequently seen in patients with CGD (Anjani et al., 2019; Winkelstein et al., 2000; de Oliveira-Junior et al., 2015; Song et al., 2011). Nevertheless, patients with classic CGD typically suffer from invasive, life-threatening, recurrent infections with specific bacteria and fungi, such as *Burkholderia cepacia*, *Staphylococcus* spp., and *Aspergillus* spp., due

to defective ROS production in all phagocytic cells (de Oliveira-Junior et al., 2015; Marciano et al., 2015; Winkelstein et al., 2000).

The infectious phenotype observed in our cohort of PKC $\delta$ -deficient patients was milder than that observed in classic CGD. Like patients with CGD or X-linked recessive Mendelian susceptibility to mycobacterial disease (MSMD) due to hypomorphic mutations of *CYBB*, PKC $\delta$ -deficient patients can suffer from BCG disease, with incomplete penetrance (Conti et al., 2016; Norouzi et al., 2012; Bustamante et al., 2011). However, whereas patients with classic CGD or p40<sup>phox</sup> deficiency do not seem to have any particular predisposition to severe viral illnesses, five PKC $\delta$ -deficient patients (P1, P2, P3, P10, and P15) presented with EBV, CMV, papillomavirus, SARS-CoV-2, and varicella-zoster virus infections, respectively (Meyts et al., 2021; Kuehn et al., 2013; Omarjee et al., 2019). Furthermore, none of the reported p40<sup>phox</sup>-deficient patients suffered from any severe invasive bacterial or fungal infections, whereas PKC $\delta$ -deficient patients did not present with any of the cutaneous infections typically seen in patients with p40<sup>phox</sup> deficiency (Li et al., 2016; van de Geer et al., 2018; Wright et al., 2019; Matute et al., 2009). Interestingly, p40<sup>phox</sup>-deficient patients, who have low to normal levels of ROS production in neutrophils and monocytes following phorbol ester stimulation, have no detectable impairment of ROS production by MDMs and MDDCs (van de Geer et al., 2018; Wright et al., 2019; Matute et al., 2009). Unlike patients with classic CGD, PKC $\delta$ -deficient patients displayed residual ROS production by circulating and monocyte-derived phagocytes, possibly accounting for the milder clinical phenotype of these patients than of patients with CGD (van de Geer et al., 2018; Matute et al., 2009; Song et al., 2011). The differences in clinical presentation between patients with PKC $\delta$  deficiency, p40<sup>phox</sup> deficiency, and classic CGD can be also explained by the mechanisms proposed here, according to which the PKC $\delta$ -dependent phosphorylation not only of p40<sup>phox</sup>, but also of p47<sup>phox</sup>, is required for ROS production. Finally, the greater susceptibility to viral illnesses observed in PKC $\delta$ -deficient patients may result from low levels of NK cell cytolytic activity, as previously shown (Kuehn et al., 2013; Kiykim et al., 2015).

One of the limitations of our study is the small size of the cohort of PKC $\delta$ -deficient patients followed over a short period. Studies of a larger number of patients are required to improve comparisons of the immunological and clinical features of PKC $\delta$  deficiency, p40<sup>phox</sup> deficiency, and classic and variant CGD (Royer-Pokora et al., 1986; Dinauer et al., 1987). Nevertheless, our data indicate that *PRKCD* mutations underlie a new, “syndromic form” of CGD, characterized by susceptibility to some, but not all, of the infections typical of CGD, associated with early-onset SLE. Indeed, the most striking phenotype observed in PKC $\delta$ -deficient patients is the early onset of SLE, which was diagnosed in 13 patients of this cohort (P1–P13), with two others presenting signs of autoimmunity (P14 and P15) and two displaying no autoimmune phenotype at the ages of 3 (P16) and 5 (P17) yr (Kuehn et al., 2013; Belot et al., 2013; Kiykim et al., 2015; Salzer et al., 2013; Lei et al., 2018; Nanthapaisal et al., 2017; Meyts et al., 2021; Sharifinejad et al., 2020; unpublished data). Several monogenic disorders underlying SLE have been reported,

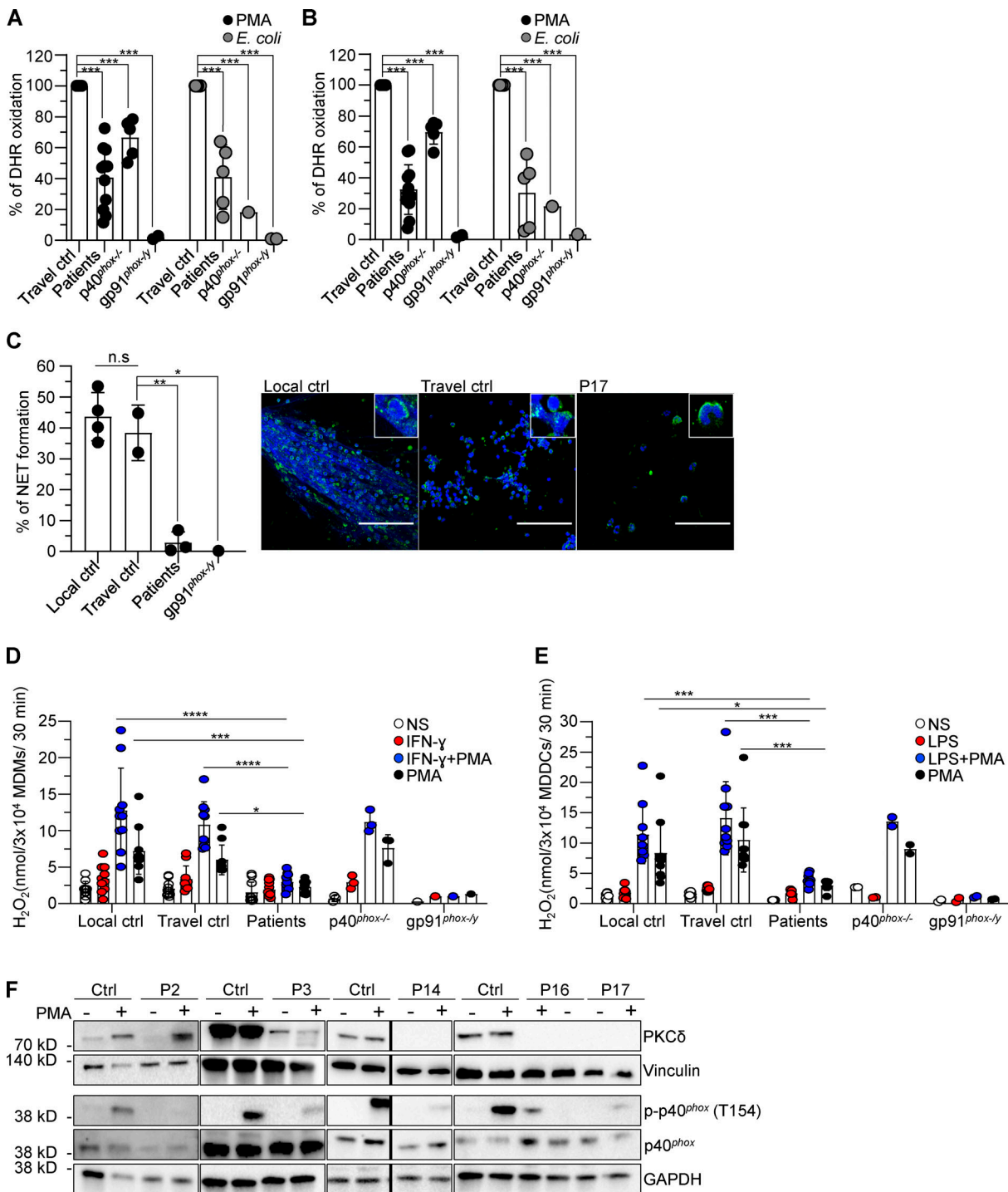


**Figure 7. NADPH oxidase activity in primary phagocytic cells from PKC $\delta$ -deficient patients. (A)** Neutrophil intracellular ROS production, as measured by DHR, upon PMA stimulation, for travel controls (ctrl;  $n = 11$ ), PKC $\delta$ -deficient patients ( $n = 11$ ), p40<sup>phox</sup>-deficient patients ( $n = 5$ ), and gp91<sup>phox</sup>-deficient patients ( $n = 2$ ), or upon *E. coli* stimulation, for travel controls ( $n = 5$ ), PKC $\delta$ -deficient patients ( $n = 5$ ), p40<sup>phox</sup>-deficient patients ( $n = 1$ ), and gp91<sup>phox</sup>-deficient patients ( $n = 2$ ). **(B)** Monocyte intracellular ROS production, measured by DHR, upon PMA stimulation, for travel controls ( $n = 11$ ), PKC $\delta$ -deficient patients ( $n = 11$ ), p40<sup>phox</sup>-deficient patients ( $n = 5$ ), and gp91<sup>phox</sup>-deficient patients ( $n = 2$ ), or upon *E. coli* stimulation, for travel controls ( $n = 5$ ), PKC $\delta$ -deficient patients ( $n = 5$ ), p40<sup>phox</sup>-deficient patients ( $n = 1$ ), and gp91<sup>phox</sup>-deficient patients ( $n = 1$ ), and gp91<sup>phox</sup>-deficient patients ( $n = 1$ ). All values are expressed as a percentage of DHR oxidation normalized against travel controls. **(C)** Left: Quantification of NET formation for healthy controls ( $n = 6$ ), PKC $\delta$ -deficient patients ( $n = 3$ ), and a gp91<sup>phox</sup>-deficient patient, after PMA stimulation. All values are expressed as a percentage of NET-forming cells. Right: Representative images of PMA-induced NET formation by neutrophils of local and travel controls and a PKC $\delta$ -deficient patient (P17). Green represents myeloperoxidase, and blue, DNA (DAPI). Scale bar = 60  $\mu$ m. **(D)** Extracellular H<sub>2</sub>O<sub>2</sub> production in response to stimulation with IFN- $\gamma$ , PMA, or both (mean  $\pm$  SD) for MDMs from local controls ( $n = 10$ ), travel controls ( $n = 10$ ), PKC $\delta$ -deficient patients ( $n = 12$ ), p40<sup>phox</sup>-deficient patients ( $n = 3$ ), and gp91<sup>phox</sup>-deficient patients ( $n = 1$ ). **(E)** Extracellular H<sub>2</sub>O<sub>2</sub> production in response to stimulation with LPS, PMA, or both (mean  $\pm$  SD), in MDDCs from local controls ( $n = 10$ ), travel controls ( $n = 10$ ), PKC $\delta$ -deficient patients ( $n = 8$ ), p40<sup>phox</sup>-deficient patients ( $n = 2$ ), and

gp91<sup>phox</sup>-deficient patients ( $n = 2$ ). (F) Western blot of MDMs of healthy controls ( $n = 4$ ) and PKC $\delta$ -deficient patients ( $n = 5$ ), without (-) or with (+) PMA stimulation. Solid bars between blots indicate different regions of the same membrane. In A–E, dots represent individual samples, and bars, the mean and SD. Two-way ANOVA was used in A–D; one-way ANOVA was used in C; \*,  $P < 0.05$ ; \*\*,  $P < 0.01$ ; \*\*\*,  $P < 0.001$ ; \*\*\*\*,  $P < 0.0001$ .

affecting the complement system, type I IFN immunity, nucleic acid metabolism, or B cell development checkpoints (Costa-Reis and Sullivan, 2017; Rahman and Isenberg, 2008; Omarjee et al., 2019). B cell development is tightly regulated to prevent self-reactivity, as B cell receptor diversification inevitably results in some B cell receptors recognizing self-antigens (Meffre and Wardemann, 2008). Autoreactive B cells are eliminated through multiple steps during B cell development. PKC $\delta$  plays a key role in regulating B cell survival, differentiation, and apoptosis (Guo et al., 2004; Griner and Kazanietz, 2007). As previously shown in mice, human PKC $\delta$  deficiency may underlie autoimmunity due to defective proapoptotic signaling during B cell development (Mecklenbräuer et al., 2002, 2004; Limnander et al., 2014).

Intriguingly, some SLE manifestations are also observed in some patients with p40<sup>phox</sup> deficiency or classic CGD (van de Geer et al., 2018; Xie et al., 2016; Parvaneh et al., 2014). Despite the overlap between the cellular phenotypes of these conditions and that of PKC $\delta$  deficiency in terms of ROS production, the SLE-like manifestations in these other conditions may be unrelated to the role of PKC $\delta$  in B cell checkpoints. SLE is often associated with an increase in type I IFN activity and a dysregulation of type I IFN metabolism (Crow, 2011; Picard and Belot, 2017; Rönnblom et al., 1990). In the absence of NADPH oxidase activity, the mitochondrial ROS-dependent NET-osis of low-density granulocytes leads to the externalization of proinflammatory oxidized mitochondrial DNA and the subsequent activation of type I IFN synthesis (Lood et al., 2016). Enhanced type I IFN activity may, therefore, contribute to the SLE-like phenotype observed in patients with impaired NADPH oxidase activity. Overall, the autoimmunity observed in PKC $\delta$ -deficient patients is probably mostly due to the defective selection of autoreactive B cells, although defective ROS production may also be involved.

## Materials and methods

### Clinical information for the newly identified patients

P13 (kindred H, II.1) was born in 2007 to nonconsanguineous parents of Turkish origin. She was vaccinated with BCG, on the left shoulder, at the age of 2 mo and developed BCG-itis 3 mo later. An excisional biopsy of the left axillary lymph node was performed, and *M. tuberculosis* PCR and culture were negative. At the age of 11 mo, P13 presented with fever and left axillary, retroauricular, and cervical lymphadenopathies. *Salmonella* sp. was documented in blood cultures and treated with ceftriaxone for 21 d. The axillary lymph node was removed; histological examination revealed necrotizing granulomatous inflammation, and *Mycobacterium bovis*-BCG was identified by culture. Serological tests for HIV were negative. The patient was treated with triple antimycobacterial therapy and was diagnosed with MSMD. Whole-blood activation tests showed that the production of IFN- $\gamma$  and IL-12p40 in response to stimulation with BCG + IL-12 and BCG +

IFN- $\gamma$  was normal. At 18 mo of age, P13 presented with a skin rash, joint pain, and high ANA levels. Drug-induced lupus erythematosus was suspected on clinical grounds, and isoniazid was discontinued. However, physical examination showed a worsening of her condition, with the appearance of lupus-like symptoms (arthralgia, morning stiffness, and limitation of movement). At the age of 24 mo, antimycobacterial treatment was discontinued. Leukocyte, absolute neutrophil, and absolute lymphocyte counts were normal. Serum IgG levels were low, whereas serum IgA, IgM, and IgE levels were within normal ranges. The immunophenotyping of B cell subsets showed predominantly high naive B cell and low memory B cell counts, with markedly high levels of CD21<sup>low</sup> and transitional B cells. In summary, this patient received multiagent antituberculosis treatment for 33 mo, without relapse or the use of other antimycobacterial treatments. The patient has had recurrent gingivitis since the age of 6 yr and, at the age of 7 yr, presented with inguinal lymphadenitis, leading to the detection of *S. aureus* by culture. The patient is now 14 yr old and remains free from mycobacterial and other infectious diseases. However, SLE and the high levels of ANA persist.

P14 and P15 (kindred I, II.1 and II.2) were born in 2010 and 2013, respectively, to nonconsanguineous parents of Turkish origin. Both were vaccinated with BCG at 1 mo of age and developed BCG-itis 6 mo later. P14 presented with fever, diarrhea, hepatosplenomegaly, failure to thrive, and left axillary lymphadenopathy with purulent discharge. Lymph node biopsy showed granulomatous inflammation with no microbial cause identified upon culture. Similarly, P15 developed left axillary lymphadenopathy and hepatosplenomegaly after BCG vaccination. Both patients were treated with isoniazid and rifampicin for 4 (P14) and 5 (P15) yr; P15 also received IVIG treatment. Prophylaxis was not indicated in P14. Both patients had high levels of ANA and developed autoimmune anemia, with no other lupus-like symptoms. Both patients are currently well.

P16 and P17 (kindred J, II.2 and II.1) were born in 2017 and 2014, respectively, to consanguineous parents of Iranian origin. Both were vaccinated with BCG at birth, but only P16 developed BCG-itis; her brother (P17) remained asymptomatic. P16 presented at 14 mo of age with bilateral anterior and posterior cervical adenopathies and mild hepatosplenomegaly. Lymph node biopsy showed chronic granulomatous inflammation with caseating necrosis. No microbe was identified, but a purified protein derivative skin test was positive. The patient received triple antimycobacterial therapy (isoniazid, rifampin, and azithromycin) for 6 mo until the adenopathies disappeared. Her serum IgG, IgA, and IgM levels were within the normal range, but her antibody responses to tetanus and diphtheria vaccines were nonprotective (anti-tetanus antibodies, 0.04 mg/dl; anti-diphtheria antibodies, 0.04 mg/dl [normal >0.1 mg/dl]). P16 and P17 both tested negative for autoantibodies and have not yet developed any lupus-like symptoms. Both patients are well, without prophylaxis.

Table 2. Summary of the functional studies in the patients' cells

Patient (kindred)	Mutation	PKC $\delta$ expression	p40 <sup>phox</sup> phosphorylation	ROS production in circulating phagocytes	ROS production in monocyte-derived cells
P1 (A)	p.R614W/p.R614W	Impaired (EBV-B cells)	Impaired after PMA and Pansorbin (EBV-B cells)	NT	Impaired after PMA, PMA + IFN- $\gamma$ and PMA + LPS (MDMs and MDDCs)
P2 (B)	p.G248S/p.G248S	Normal (EBV-B cells and MDMs)	Impaired after PMA and Pansorbin (EBV-B cells and MDMs)	Impaired after PMA (neutrophils and monocytes)	Impaired after PMA, PMA + IFN- $\gamma$ and PMA + LPS (MDMs and MDDCs)
P3 (C)	p.G510S/p.G510S	Impaired (EBV-B cells, neutrophils, and MDMs)	Impaired after PMA and Pansorbin (EBV-B cells and MDMs)	Impaired after PMA and <i>E. coli</i> (neutrophils and monocytes)	Impaired after PMA, PMA + IFN- $\gamma$ and PMA + LPS (MDMs and MDDCs)
P4 (C)	p.G510S/p.G510S	NT	NT	NT	NT
P5 (C)	p.G510S/p.G510S	Impaired (EBV-B cells)	Impaired after PMA and Pansorbin (EBV-B cells)	Impaired after PMA (neutrophils and monocytes)	Impaired after PMA, PMA + IFN- $\gamma$ and PMA + LPS (MDMs and MDDCs)
P6 (D)	c.1352 + 1G>A/c.1352 + 1G>A	Abolished (EBV-B cells)	Impaired (EBV-B cells)	Impaired after PMA (neutrophils and monocytes)	Impaired after PMA, PMA + IFN- $\gamma$ and PMA + LPS (MDMs and MDDCs)
P7 (E)	p.G432W	NT	NT	NT	NT
P8 (E)	p.G432W	NT	NT	NT	NT
P9 (E)	p.G432W	NT	NT	NT	NT
P10 (F)	c.788-2A>G/p.Q191*	Abolished (EBV-B cells)	Impaired after PMA and Pansorbin (EBV-B cells)	Impaired after PMA (neutrophils and monocytes)	Impaired after PMA, PMA + IFN- $\gamma$ and PMA + LPS (MDMs and MDDCs)
P11 (F)	c.788-2A>G/p.Q191*	Abolished (EBV-B cells)	Impaired after PMA and Pansorbin (EBV-B cells)	Impaired after PMA (neutrophils and monocytes)	Impaired after PMA, PMA + IFN- $\gamma$ and PMA + LPS (MDMs and MDDCs)
P12 (G)	c.1293_1294insA/c.1293_1294insA	NT	NT	NT	NT
P13 (H)	c.571 + 2dup/c.571 + 2dup	Abolished (EBV-B cells, neutrophils, monocytes, and MDMs)	Impaired after PMA and Pansorbin (EBV-B cells)	Impaired after PMA (neutrophils and monocytes)	Impaired after PMA, PMA + IFN- $\gamma$ and PMA + LPS (MDMs and MDDCs)
P14 (I)	c.1384C>T/c.1384C>T	Abolished (MDMs)	Impaired (MDMs)	Impaired after PMA and <i>E. coli</i> (neutrophils and monocytes)	Impaired after PMA and PMA + IFN- $\gamma$ (MDMs)
P15 (I)	c.1384C>T/c.1384C>T	NT	NT	Impaired after PMA and <i>E. coli</i> (neutrophils and monocytes)	Impaired after PMA and PMA + IFN- $\gamma$ (MDMs)
P16 (J)	c.642del/c.642del	Abolished (MDMs)	Impaired (MDMs)	Impaired after PMA and <i>E. coli</i> (neutrophils and monocytes)	Impaired after PMA and PMA + IFN- $\gamma$ (MDMs)
P17 (J)	c.642del/c.642del	Abolished (MDMs)	Impaired (MDMs)	Impaired after PMA and <i>E. coli</i> (neutrophils and monocytes)	Impaired after PMA and PMA + IFN- $\gamma$ (MDMs)

Functional results obtained in cell lines (EBV-B cells) or primary cells (neutrophils, monocytes, MDMs, and MDDCs). EBV-B cells, EBV-immortalized B cells; NT, not tested.

### Blood collection

Blood samples were collected from all patients and relatives, at the local institutions, after written informed consent had been obtained. The study was approved by the institutional review boards of the Institut National de la Santé et de la Recherche Médicale (INSERM), Rockefeller University, and Necker Hospital for Sick Children. All these procedures were conducted in accordance with the 1975 Declaration of Helsinki, as revised in 2013.

### Molecular genetics

For P13, genomic DNA (gDNA) was isolated from whole blood with the iPrep PureLink gDNA Blood Kit and iPrep Instruments (Life Technologies, Thermo Fisher Scientific). Exome capture was performed with the SureSelect Human All Exon 71 Mb kit (Agilent Technologies), with 3  $\mu$ g gDNA. Single-end sequencing was performed on an Illumina Genome Analyzer IIx (Illumina). For P14 and P15, gDNA was obtained from the patients' peripheral blood

samples with the QIAamp DNA Blood Mini QIAcube Kit (Qiagen). The library was constructed with a 200-amplitude primary immunodeficiency panel kit from Sistemas Genomicos. Samples and index reading primers were loaded into a 300-cycle MiSeq Reagent Kit v2 300 cartridge (Illumina), and parallel sequencing was performed in MiSeq v2 Flowcell (Illumina). The variants of all the other patients were identified by WES (P1, P2, P3, P6, P7, P12, P16, and P17), Sanger sequencing (P4, P5, P8, and P9), or focused WES with a primary immunodeficiency subpanel for next-generation sequencing (P10–P11), as previously described (Kuehn et al., 2013; Kiykim et al., 2015; Belot et al., 2013; Salzer et al., 2013; Lei et al., 2018; Nanthapaisal et al., 2017; Sharifinejad et al., 2020). All mutations and familial segregation patterns were confirmed by amplifying the flanking regions of the variants obtained with specific primers (Table S1). PCR products were analyzed by electrophoresis in 1% agarose gels, sequenced with the Big Dye Terminator v3.1 cycle sequencing kit (Applied Biosystems), and analyzed on an ABI Prism 3700 (Applied Biosystems). The patients reported here did not consent to the deposition of their genomic data.

### Expression of mutated PKC $\delta$ proteins in transfected HEK293T cells

Site-directed mutagenesis with specific primers (Table S2) was performed to generate the *PRKCD* variants in the pCMV6-*PRKCD*-WT-DDK plasmid (#RC221652; OriGene). HEK293T cells were transfected with 1  $\mu$ g of the plasmid in the presence of X-tremeGENE 9 DNA transfection reagent (Merck) for 24 h. Protein extraction and Western blotting were performed as described below.

### TOPO-TA cloning

RNA was extracted from the EBV-B cells of P2, P6, P10, P11, P13, and a healthy control with the Quick-RNA Microprep Kit (Zymo Research), and RNA was transcribed to generate cDNA with the High-Capacity RNA-to-cDNA Kit (Thermo Fisher Scientific). Full-length *PRKCD* cDNA was amplified by PCR with the following primers: 5'-CTATGAGCTGGGCTCCCTG-3' and 5'-CCAGGAGGTGCTCGAATTTG-3'. The purified PCR products were inserted into a pCR4-TOPO vector (Thermo Fisher Scientific) and used to transform competent NEB 10- $\beta$  *E. coli* cells (New England Biolabs). We picked 100 single colonies per reaction, and the inserted cDNA was amplified with M13 forward and reverse primers.

### RT-qPCR

Gene expression was analyzed by RT-qPCR with the TaqMan Universal PCR Master Mix (Thermo Fisher Scientific) and TaqMan probes for *PRKCD* (Hs01090047\_m1 and Hs01090051\_m1) and *GUSB* (4326320E; all from Thermo Fisher Scientific). Gene expression was normalized against *GUSB* as an endogenous control for each sample and then according to the mean value for controls in one experiment.

### Western blot analysis

EBV-B cells were treated with 400 ng/ml PMA (Sigma-Aldrich) or 2 mg/ml Pansorbin (Sigma-Aldrich) in HBSS for 30 min or were left untreated, and total protein extracts were prepared with insoluble protein buffer (20 mM Tris-HCl, pH 8, 150 mM NaCl, 1 mM EDTA, and 1% Triton X-100, supplemented with 1 mM 4-[2-aminoethyl] benzene sulfonyl fluoride hydrochloride, 20 ng/ml

chymostatin, 10 nM leupeptin, and 2 mM PMSF; all from Sigma-Aldrich). Protein extracts (30  $\mu$ g protein per lane) were resolved by electrophoresis in a 10% Criterion TGX precast gel, and the bands obtained were transferred onto a nitrocellulose membrane by standard transfer methods, in a Transblot turbo system (Bio-Rad). Membranes were probed by overnight incubation with the appropriate primary antibodies (Table S3) at 4°C. After incubation with the corresponding secondary antibody (goat anti-rabbit IgG (H+L)-HRP and goat anti-mouse IgG (H+L)-HRP; Bio-Rad), proteins were detected by chemiluminescence. For the quantification of PKC $\delta$  protein, membranes were probed with anti-PKC $\delta$  and anti-GAPDH antibodies, and binding was visualized with the Odyssey CLx Imaging system (LI-COR) after incubation with IR-Dye 800CW goat anti-mouse IgG (H+L) and IRDye 680RD goat anti-rabbit IgG (H+L; both LI-COR) secondary antibodies.

### Flow cytometry

EBV-B cells were incubated with LIVE/DEAD Fixable Aqua Dead Cell Stain (Thermo Fisher Scientific) for 10 min at 37°C. Cells were fixed and permeabilized in intracellular fixation and permeabilization buffer (eBioscience, Thermo Fisher Scientific) for 30 min. Intracellular staining was performed for 30 min at 4°C with the appropriate antibodies (Table S3). Cells were analyzed by flow cytometry with a Gallios FACS Analyzer.

### Coimmunoprecipitation

Coimmunoprecipitation was performed as previously described (Béziat et al., 2018). Briefly, HEK293T cells were cotransfected with constructs encoding Myc-tagged, DDK-tagged, or V5-tagged proteins or the empty pCMV6 or pCDNA3.1 plasmid in the presence of X-tremeGENE 9 DNA transfection reagent. After 24 h, cells were lysed with lysis buffer (50 mM Tris, pH 7.4, 150 mM NaCl, 2 mM EDTA, and 0.5% Triton X-100) supplemented with aprotinin (10  $\mu$ g/ml; Sigma Aldrich), PMSF (1 mM), and leupeptin (10  $\mu$ g/ml) for 30 min at 4°C and centrifuged for 5 min at 16,000  $\times$ g. The supernatant was collected for immunoprecipitation. Immunoprecipitation was performed with anti-V5 (#R96025; Thermo Fisher Scientific) or anti-DDK (#OT14C5; OriGene) antibodies and agarose-A/G beads (Santa Cruz Biotechnology), after a background clearing step with a normal mouse IgG antibody (#sc-2025; Santa Cruz Biotechnology) and agarose-A/G beads. Total and immunoprecipitated proteins were then analyzed by Western blotting, as described above.

### Apoptosis measurement

We used  $1 \times 10^5$  EBV-B cells to inoculate RPMI 1640 containing 10% FCS in the presence or absence of PMA (100 ng/ml) or APO-1-1 (1  $\mu$ g/ml; Enzo Life Science), in triplicate, in 96-well plates. The cells were cultured for 24 h at 37°C. Cells were stained with LIVE/DEAD Fixable Aqua Dead Cell Stain, and live cells were counted by flow cytometry with constant time acquisition on a Gallios FACS Analyzer. The percentage of live cells was calculated as previously described (Kuehn et al., 2013).

### Retroviral transduction of EBV-B cells

Retrovirus-mediated transduction was performed as previously described (Martínez-Barricarte et al., 2016). In brief, the coding

sequences of the *PRKCD* WT and *PRKCD* mutant alleles were inserted into the pLZRS-IRES-ANGFR plasmid. Retroviruses were produced by transfecting Phoenix A cells with the newly generated plasmids, and EBV-B cells from PKC $\delta$ -deficient patients were transduced with the viral concentrate obtained. The transduced cells were subjected to magnetic activated cell sorting purification with anti-CD271 MicroBeads (Miltenyi Biotec), and purified cells were used in subsequent experiments. Transduction was confirmed by flow cytometry with anti-CD271-PE antibody (BD Bioscience).

### Differentiation of MDMs and MDDCs

MDMs and MDDCs were differentiated as previously described (van de Geer et al., 2018; Bustamante et al., 2011; Conti et al., 2015). In brief, CD14<sup>+</sup> cells were isolated from peripheral blood mononuclear cells by positive selection with anti-CD14 MicroBeads (Miltenyi Biotec). For MDM differentiation, cells were cultured in RPMI 1640 containing 10% FCS and M-CSF (50 ng/ml). On day 7, IL-4 (50 ng/ml) was added, and the cells were incubated for a further 7 d for the completion of differentiation. MDDCs were obtained by incubation in the presence of GM-CSF (50 ng/ml) and IL-13 (20 ng/ml; all R&D Systems) for 7 d.

### NADPH oxidase functional assays

The intracellular production of O<sub>2</sub><sup>-</sup> in EBV-B cells was assessed by chemiluminescence (Sigma-Aldrich; van de Geer et al., 2018). We stimulated 5 × 10<sup>5</sup> cells with PMA (400 ng/ml) or heat-killed *S. aureus* cells (Pansorbin, 2 mg/ml; Sigma-Aldrich) and light production was monitored every 5 min with a Victor X4 plate reader. NADPH oxidase activity was assessed in EBV-B cells, MDMs, and MDDCs by measuring extracellular H<sub>2</sub>O<sub>2</sub> release with an Amplex Red Kit (Thermo Fisher Scientific), as previously described (van de Geer et al., 2018; Bustamante et al., 2011; Conti et al., 2015). In brief, 3 × 10<sup>4</sup> cells were stimulated with PMA (400 ng/ml), and H<sub>2</sub>O<sub>2</sub> release was quantified with a Victor X4 plate reader (PerkinElmer). MDMs or MDDCs were cultured for 16 to 18 h before the experiment, in the presence of 5 × 10<sup>3</sup> IU/ml IFN- $\gamma$  (Imukin, Boehringer Ingelheim) or 1  $\mu$ g/ml LPS (*Salmonella minnesota*; Sigma-Aldrich), respectively. ROS production by neutrophils and monocytes was quantified with the Burstest (Phagoburst kit; BD) containing PMA and opsonized *E. coli* bacteria. The assay was performed according to the manufacturer's instructions, and the amount of rhodamine 123 (mean fluorescence intensity) was assessed by flow cytometry with a Gallios FACS Analyzer. DHR oxidation is expressed as a percentage of the rhodamine 123 produced by the corresponding travel controls.

### NET formation

Neutrophils were isolated from whole blood with density gradient centrifugation and Polymorphprep (Progen). We used 1 × 10<sup>5</sup> neutrophils to seed 8-well microslides (Ibidi), which were then incubated at 37°C for 15 min. PMA (100 ng/ml) was then added, and the cells were incubated for 3 h at 37°C. The cells were fixed by incubation in 4% paraformaldehyde for 15 min, blocked and permeabilized by incubation with 5% BSA in PBS-Tween for 1 h, and incubated overnight with an anti-myeloperoxidase antibody (ab45977; Abcam). Secondary staining was performed by incubation for 1 h with a goat anti-rabbit Alexa Fluor 488 antibody (Thermo Fisher Scientific). Cells were mounted in ProLong Gold antifade reagent containing DAPI

(Thermo Fisher Scientific), and images were acquired at the Necker Institute Imaging Facility with a Leica SP8 gSTED confocal microscope (Leica). Percentage NET formation was quantified by counting cells with decondensed nuclei and extracellular DAPI-positive fibers in at least five image fields selected at random.

### Statistics

A linear mixed model was used to analyze the data presented in Fig. 3 D, to take repeated measurements into account. The null hypothesis was that the distribution of EBV-B cell survival rates after PMA or APO stimulation was similar in patients and controls. The null hypothesis was rejected if the P value was <0.05.

Statistical analysis and visualization of results for Fig. 7, A–E, were performed using GraphPad Prism 8.4.3. For Fig. 7, A, B, D, and E, two-way ANOVA with Tukey's multiple comparison was performed. One-way ANOVA was performed for Fig. 7 C. A P value <0.05 was considered statistically significant.

### Online supplemental material

Fig. S1 shows evolutionary conservation of the missense variants and splicing consequences of the variants affecting splice sites. Fig. S2 shows decreased phosphorylation of MARCKS in the patients' EBV-B cells. Fig. S3 presents the complementation of the patients' EBV-B cells with WT *PRKCD*. Fig. S4 provides additional information about the NADPH oxidase subunit expression and their interaction with PKC $\delta$ . Fig. S5 presents additional evidence of impaired ROS production in the patients' primary cells including ROS production in neutrophils and monocytes, NET formation and phosphorylation of p47<sup>phox</sup>. Table S1, Table S2, and Table S3 provide primer sequences for sequencing and site-directed mutagenesis, and antibody references.

### Acknowledgments

This paper is dedicated to the memory of Prof. Asghar Aghamohammadi, who passed away in November 2020, and made immense contributions to the understanding and treatment of primary immunodeficiencies.

We thank all patients, their relatives, and the treatment teams for their cooperation in this study. We thank all the members of the Laboratory of Human Genetics of Infectious Diseases for helpful discussions. We also thank Christine Rivalain, Cécile Pattissier, Lazaro Lorenzo-Diaz, Dominick Papandrea, Dana Liu, and Yelena Nemirovskaya for administrative assistance and Gaspard Kerner for statistical advice. We thank the Necker Institute Imaging Facility for technical advice. The graphical abstract was created with BioRender.com under subscription.

This research was supported by the Yale Center for Mendelian Genomics funded by the National Human Genome Research Institute (UMIHG006504). The Howard Hughes Medical Institute laboratory was funded in part by the National Institute of Allergy and Infectious Diseases (grants 5R01AI089970, 5R37AI095983, and R01AI127564-01), the National Center for Research Resources, and the National Center for Advancing Translational Sciences of the National Institutes of Health (grant 8UL1TR001866 for J-L. Casanova), the Rockefeller University, the St. Giles Foundation, INSERM, the University of Paris, the French Foundation for Medical

Research (EQU201903007798), the Integrative Biology of Emerging Infectious Diseases Laboratory of Excellence (ANR-10-LABX-62-IBRID), the SCOR Corporate Foundation for Science, and the French National Research Agency (ANR) under the “Investments for the future” program (grant ANR-10-IAHU-01), ANR-IFNPHOX (grant ANR-13-ISV3-0001-01 for J. Bustamante), ANR-GENMSMD (grant ANR-16-CE17-0005-01 for J. Bustamante), ANR-GENCMCD (grant ANR-11-BSV3-005-01 for A. Puel), and ANR-HGDIFD (grant ANR-14-CE15-0006-01 for J. Bustamante). A-L. Neehus was supported by the Bettencourt Schueller Foundation and the International PhD program of the Imagine Institute, K. Moriya by a Japanese Foundation for Pediatric Research fellowship grant and EURO-CMC project (grant ANR-14-RARE-0005-02 for J. Bustamante), R. Lévy by the Société Nationale Française de Médecine Interne (Bourse Marcel Simon), the INSERM PhD program for medical doctors (poste d'accueil INSERM), and the Fulbright grant (Franco-American commission), T. Le Voyer by the Bettencourt Schueller Foundation and the MD-PhD program of Imagine Institute, and A. Nieto-Patlán by the Consejo Nacional de Ciencia y Tecnología National PhD Fellowship Program. All research at the Great Ormond Street Hospital National Health Service Foundation Trust is supported by the National Institute for Health Research Biomedical Research Centre. P.A. Brogan also acknowledges support from the Great Ormond Street Hospital Charity. N. Lachmann acknowledges support from the Deutsche Forschungsgemeinschaft under Germany's Excellence Strategy - EXC 2155 - project number 390874280 and the REBIRTH Center for Translational Regenerative Medicine funded through the State of Lower Saxony (MWK: ZN3440).

Author contributions: A-L. Neehus, J-L. Casanova, A. Puel, and J. Bustamante conceived and designed the study. A-L. Neehus, K. Moriya, T. Le Voyer, A. Nieto-Patlán, R. Lévy, M. Roynard, K. Haake, M. Migaud, and K. Dorgham performed the experiments. A. Özen, E. Karakoc-Aydiner, S. Baris, A. Yildiran, E. Altundag, F. Dogu, S. Has-kologlu, E. İnce, G. Uzel, A. Kiykim, K. Boztug, M.R. Roderick, M. Shahroei, P.A. Brogan, H. Abolhassani, G. Hancioglu, N. Parvaneh, A. Belot, and A. Ikinciogullari were the treating physicians responsible for clinical diagnosis, deep phenotyping, sample collection, and patient follow-up. G. Gorochov, L. Abel, N. Lachmann, J. El-Benna, and A. Belot provided conceptual advice. A-L. Neehus, J-L. Casanova, A. Puel, and J. Bustamante analyzed the results and wrote the manuscript. All authors revised the manuscript and approved the final manuscript as submitted.

Disclosures: P.A. Brogan reported personal fees from Sobi, Novartis, Roche, and GSK, and grants from Sobi outside the submitted work. No other disclosures were reported.

Submitted: 2 March 2021

Revised: 14 May 2021

Accepted: 21 June 2021

## References

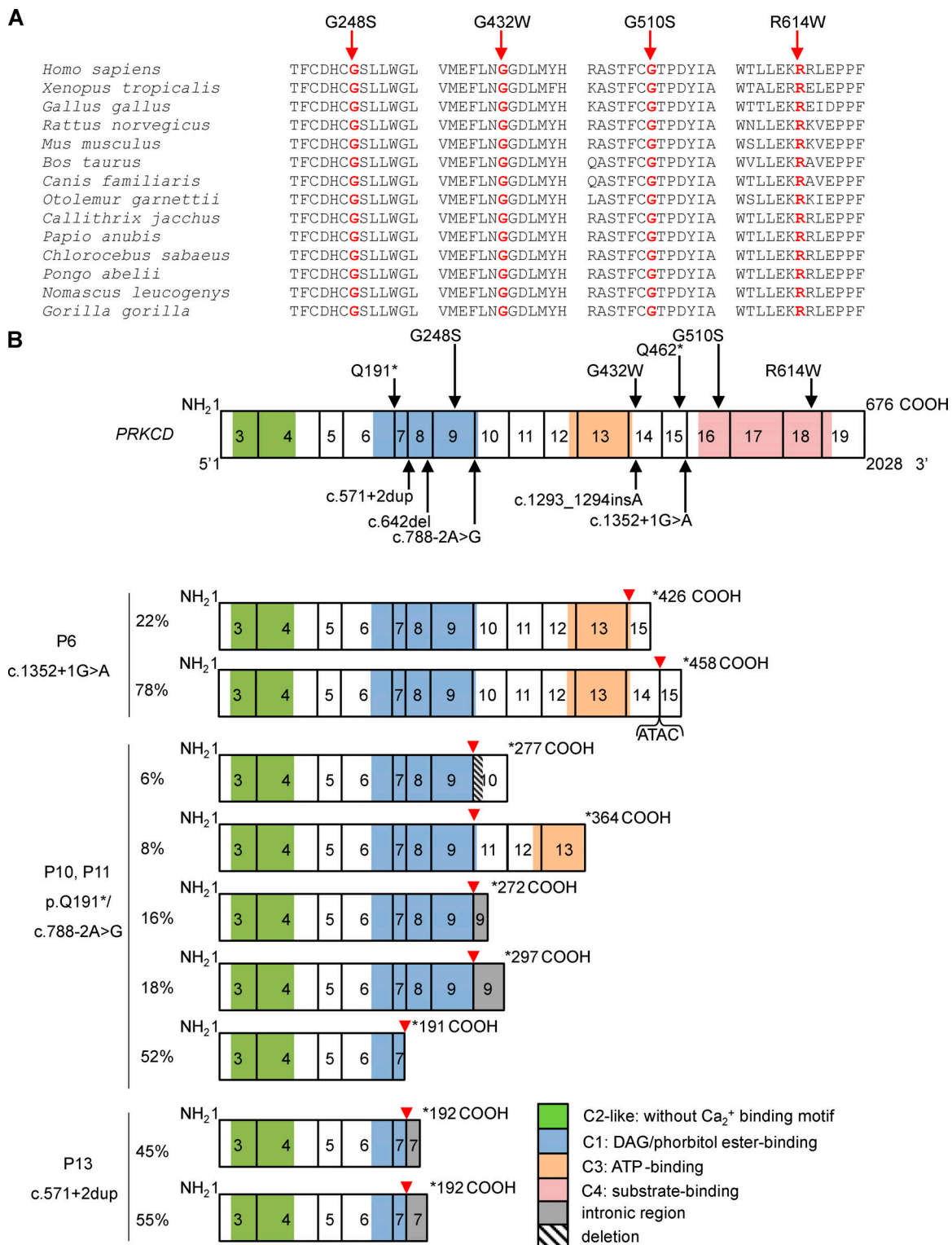
- Anjani, G., P. Vignesh, V. Joshi, J.K. Shandilya, D. Bhattarai, J. Sharma, and A. Rawat. 2019. Recent advances in chronic granulomatous disease. *Genes Dis.* 7:84–92. <https://doi.org/10.1016/j.gendis.2019.07.010>
- Basu, A., and D. Pal. 2010. Two faces of protein kinase C $\delta$ : the contrasting roles of PKC $\delta$  in cell survival and cell death. *ScientificWorldJournal.* 10: 2272–2284. <https://doi.org/10.1100/tsw.2010.214>

- Belambri, S.A., L. Rolas, H. Raad, M. Hurtado-Nedelec, P.M.-C. Dang, and J. El-Benna. 2018. NADPH oxidase activation in neutrophils: Role of the phosphorylation of its subunits. *Eur. J. Clin. Invest.* 48(Suppl 2):e12951. <https://doi.org/10.1111/eci.12951>
- Belot, A., P.R. Kasher, E.W. Trotter, A.-P. Foray, A.-L. Debaud, G.I. Rice, M. Szykiewicz, M.-T. Zabet, I. Rouvet, S.S. Bhaskar, et al. 2013. Protein kinase c $\delta$  deficiency causes mendelian systemic lupus erythematosus with B cell-defective apoptosis and hyperproliferation. *Arthritis Rheum.* 65:2161–2171. <https://doi.org/10.1002/art.38008>
- Bey, E.A., B. Xu, A. Bhattacharjee, C.M. Oldfield, X. Zhao, Q. Li, V. Subbulakshmi, G.M. Feldman, F.B. Wientjes, and M.K. Cathcart. 2004. Protein kinase C  $\delta$  is required for p47phox phosphorylation and translocation in activated human monocytes. *J. Immunol.* 173:5730–5738. <https://doi.org/10.4049/jimmunol.173.9.5730>
- Béziat, V., J. Li, J.-X. Lin, C.S. Ma, P. Li, A. Bousfiha, I. Pellier, S. Zoghi, S. Baris, S. Keles, et al. 2018. A recessive form of hyper-IgE syndrome by disruption of ZNF341-dependent STAT3 transcription and activity. *Sci. Immunol.* 3:eaat4956. <https://doi.org/10.1126/sciimmunol.aat4956>
- Bouin, A.P., N. Grandvaux, P.V. Vignais, and A. Fuchs. 1998. p40(phox) is phosphorylated on threonine 154 and serine 315 during activation of the phagocyte NADPH oxidase. Implication of a protein kinase c-type kinase in the phosphorylation process. *J. Biol. Chem.* 273:30097–30103. <https://doi.org/10.1074/jbc.273.46.30097>
- Brown, G.E., M.Q. Stewart, H. Liu, V.-L. Ha, and M.B. Yaffe. 2003. A novel assay system implicates PtdIns(3,4)P(2), PtdIns(3)P, and PKC  $\delta$  in intracellular production of reactive oxygen species by the NADPH oxidase. *Mol. Cell.* 11:35–47. [https://doi.org/10.1016/S1097-2765\(03\)00005-4](https://doi.org/10.1016/S1097-2765(03)00005-4)
- Bustamante, J., A.A. Arias, G. Vogt, C. Picard, L.B. Galicia, C. Prando, A.V. Grant, C.C. Marchal, M. Hubeau, A. Chapgier, et al. 2011. Germline CYBB mutations that selectively affect macrophages in kindreds with X-linked predisposition to tuberculous mycobacterial disease. *Nat. Immunol.* 12:213–221. <https://doi.org/10.1038/ni.1992>
- Chessa, T.A.M., K.E. Anderson, Y. Hu, Q. Xu, O. Rausch, L.R. Stephens, and P.T. Hawkins. 2010. Phosphorylation of threonine 154 in p40phox is an important physiological signal for activation of the neutrophil NADPH oxidase. *Blood.* 116:6027–6036. <https://doi.org/10.1182/blood-2010-08-300889>
- Cho, W. 2001. Membrane targeting by C1 and C2 domains. *J. Biol. Chem.* 276: 32407–32410. <https://doi.org/10.1074/jbc.R100007200>
- Conti, F., W.C. Aragão Filho, C. Prando, C. Deswarte, M. Hubeau, P.E. Newburger, J.-L. Casanova, J. Bustamante, and A. Condino-Neto. 2015. Phagocyte nicotinamide adenine dinucleotide phosphate oxidase activity in patients with inherited IFN- $\gamma$ R1 or IFN- $\gamma$ R2 deficiency. *J. Allergy Clin. Immunol.* 135:1393–5.e1. <https://doi.org/10.1016/j.jaci.2014.11.004>
- Conti, F., S.O. Lugo-Reyes, L. Blancas Galicia, J. He, G. Aksu, E. Borges de Oliveira Jr., C. Deswarte, M. Hubeau, N. Karaca, M. de Suremain, et al. 2016. Mycobacterial disease in patients with chronic granulomatous disease: A retrospective analysis of 71 cases. *J. Allergy Clin. Immunol.* 138: 241–248.e3. <https://doi.org/10.1016/j.jaci.2015.11.041>
- Costa-Reis, P., and K.E. Sullivan. 2017. Monogenic lupus: it's all new! *Curr. Opin. Immunol.* 49:87–95. <https://doi.org/10.1016/j.coi.2017.10.008>
- Crow, Y.J. 2011. Type I interferonopathies: a novel set of inborn errors of immunity. *Ann. N. Y. Acad. Sci.* 1238:91–98. <https://doi.org/10.1111/j.1749-6632.2011.06220.x>
- de Oliveira-Junior, E.B., N.B. Zurro, C. Prando, O. Cabral-Marques, P.V.S. Pereira, L.-F. Schimke, S. Klaver, M. Buzolin, L. Blancas-Galicia, L. Santos-Argumedo, et al. 2015. Clinical and Genotypic Spectrum of Chronic Granulomatous Disease in 71 Latin American Patients: First Report from the LASID Registry. *Pediatr. Blood Cancer.* 62:2101–2107. <https://doi.org/10.1002/pbc.25674>
- DeVries-Seimon, T.A., A.M. Ohm, M.J. Humphries, and M.E. Reyland. 2007. Induction of apoptosis is driven by nuclear retention of protein kinase C delta. *J. Biol. Chem.* 282:22307–22314. <https://doi.org/10.1074/jbc.M703661200>
- Dinauer, M.C., S.H. Orkin, R. Brown, A.J. Jesaitis, and C.A. Parkos. 1987. The glycoprotein encoded by the X-linked chronic granulomatous disease locus is a component of the neutrophil cytochrome b complex. *Nature.* 327:717–720. <https://doi.org/10.1038/327717a0>
- Duquesnes, N., F. Lezoualc'h, and B. Crozatier. 2011. PKC-delta and PKC-epsilon: foes of the same family or strangers? *J. Mol. Cell. Cardiol.* 51: 665–673. <https://doi.org/10.1016/j.yjmcc.2011.07.013>
- Durgan, J., N. Michael, N. Totty, and P.J. Parker. 2007. Novel phosphorylation site markers of protein kinase C delta activation. *FEBS Lett.* 581: 3377–3381. <https://doi.org/10.1016/j.febslet.2007.06.035>
- El-Benna, J., P.M.-C. Dang, M.-A. Gougerot-Pocidallo, J.-C. Marie, and F. Braut-Boucher. 2009. p47phox, the phagocyte NADPH oxidase/NOX2 organizer: structure, phosphorylation and implication in diseases. *Exp. Mol. Med.* 41:217–225. <https://doi.org/10.3858/emm.2009.41.4.058>

- Evren, E., E. Ringqvist, and T. Willinger. 2020. Origin and ontogeny of lung macrophages: from mice to humans. *Immunology*. 160:126–138. <https://doi.org/10.1111/imm.13154>
- Fontayne, A., P.M.-C. Dang, M.-A. Gougerot-Pocidal, and J. El-Benna. 2002. Phosphorylation of p47phox sites by PKC alpha, beta II, delta, and zeta: effect on binding to p22phox and on NADPH oxidase activation. *Biochemistry*. 41:7743–7750. <https://doi.org/10.1021/bi011953s>
- Gomel, R., C. Xiang, S. Finniss, H.K. Lee, W. Lu, H. Okhrimenko, and C. Brodie. 2007. The localization of protein kinase Cdelta in different subcellular sites affects its proapoptotic and antiapoptotic functions and the activation of distinct downstream signaling pathways. *Mol. Cancer Res.* 5:627–639. <https://doi.org/10.1158/1541-7786.MCR-06-0255>
- Grandvaux, N., S. Elsen, and P.V. Vignais. 2001. Oxidant-dependent phosphorylation of p40phox in B lymphocytes. *Biochem. Biophys. Res. Commun.* 287:1009–1016. <https://doi.org/10.1006/bbrc.2001.5665>
- Griner, E.M., and M.G. Kazanietz. 2007. Protein kinase C and other diacylglycerol effectors in cancer. *Nat. Rev. Cancer*. 7:281–294. <https://doi.org/10.1038/nrc2110>
- Guo, B., T.T. Su, and D.J. Rawlings. 2004. Protein kinase C family functions in B-cell activation. *Curr. Opin. Immunol.* 16:367–373. <https://doi.org/10.1016/j.coi.2004.03.012>
- Humphries, M.J., A.M. Ohm, J. Schaack, T.S. Adwan, and M.E. Reyland. 2008. Tyrosine phosphorylation regulates nuclear translocation of PKCdelta. *Oncogene*. 27:3045–3053. <https://doi.org/10.1038/sj.onc.1210967>
- Kazanietz, M.G., S. Wang, G.W. Milne, N.E. Lewin, H.L. Liu, and P.M. Blumberg. 1995. Residues in the second cysteine-rich region of protein kinase C delta relevant to phorbol ester binding as revealed by site-directed mutagenesis. *J. Biol. Chem.* 270:21852–21859. <https://doi.org/10.1074/jbc.270.37.21852>
- Kiykim, A., I. Ogulur, S. Baris, E. Salzer, E. Karakoc-Aydiner, A.O. Ozen, W. Garncarz, T. Hirschmugl, A. Krol, A.D. Yucelten, et al. 2015. Potentially Beneficial Effect of Hydroxychloroquine in a Patient with a Novel Mutation in Protein Kinase Cδ Deficiency. *J. Clin. Immunol.* 35:523–526. <https://doi.org/10.1007/s10875-015-0178-9>
- Kuehn, H.S., J.E. Niemela, A. Rangel-Santos, M. Zhang, S. Pittaluga, J.L. Stoddard, A.A. Hussey, M.O. Evbuomwan, D.A.L. Priel, D.B. Kuhns, et al. 2013. Loss-of-function of the protein kinase C δ (PKCδ) causes a B-cell lymphoproliferative syndrome in humans. *Blood*. 121:3117–3125. <https://doi.org/10.1182/blood-2012-12-469544>
- Lachmann, N., M. Ackermann, E. Frenzel, S. Liebhaber, S. Brenning, C. Happle, D. Hoffmann, O. Klimentkova, D. Lüttge, T. Buchegger, et al. 2015. Large-scale hematopoietic differentiation of human induced pluripotent stem cells provides granulocytes or macrophages for cell replacement therapies. *Stem Cell Reports*. 4:282–296. <https://doi.org/10.1016/j.stemcr.2015.01.005>
- Lei, L., S. Muhammad, M. Al-Obaidi, N. Sebire, I.L. Cheng, D. Eleftheriou, and P. Brogan. 2018. Successful use of ofatumumab in two cases of early-onset juvenile SLE with thrombocytopenia caused by a mutation in protein kinase C δ. *Pediatr. Rheumatol. Online J.* 16:61. <https://doi.org/10.1186/s12969-018-0278-1>
- Li, W., H. Mischak, J.C. Yu, L.M. Wang, J.F. Mushinski, M.A. Heidar, and J.H. Pierce. 1994. Tyrosine phosphorylation of protein kinase C-delta in response to its activation. *J. Biol. Chem.* 269:2349–2352. [https://doi.org/10.1016/S0021-9258\(17\)41948-X](https://doi.org/10.1016/S0021-9258(17)41948-X)
- Li, X., X. Cullere, H. Nishi, G. Saggi, E. Durand, M.K. Mansour, J.M. Tam, X.Y. Song, X. Lin, J.M. Vyas, and T. Mayadas. 2016. PKC-δ activation in neutrophils promotes fungal clearance. *J. Leukoc. Biol.* 100:581–588. <https://doi.org/10.1189/jlb.4A0915-405R>
- Limnander, A., P. Depeille, T.S. Freedman, J. Liou, M. Leitges, T. Kurosaki, J.P. Roese, and A. Weiss. 2011. STIM1, PKC-δ and RasGRP set a threshold for proapoptotic Erk signaling during B cell development. *Nat. Immunol.* 12:425–433. <https://doi.org/10.1038/ni.2016>
- Limnander, A., J. Zikherman, T. Lau, M. Leitges, A. Weiss, and J.P. Roese. 2014. Protein kinase Cδ promotes transitional B cell-negative selection and limits proximal B cell receptor signaling to enforce tolerance. *Mol. Cell Biol.* 34:1474–1485. <https://doi.org/10.1128/MCB.01699-13>
- Lood, C., L.P. Blanco, M.M. Purmalek, C. Carmona-Rivera, S.S. De Ravin, C.K. Smith, H.L. Malech, J.A. Ledbetter, K.B. Elkon, and M.J. Kaplan. 2016. Neutrophil extracellular traps enriched in oxidized mitochondrial DNA are interferogenic and contribute to lupus-like disease. *Nat. Med.* 22:146–153. <https://doi.org/10.1038/nm.4027>
- Marciano, B.E., C. Spalding, A. Fitzgerald, D. Mann, T. Brown, S. Osgood, L. Yockey, D.N. Darnell, L. Barnhart, J. Daub, et al. 2015. Common severe infections in chronic granulomatous disease. *Clin. Infect. Dis.* 60:1176–1183. <https://doi.org/10.1093/cid/ciu1154>
- Martínez-Barricarte, R., S.J. de Jong, J. Markle, R. de Paus, S. Boisson-Dupuis, J. Bustamante, E. van de Vosse, B. Fleckenstein, and J.-L. Casanova. 2016. Transduction of Herpesvirus saimiri-Transformed T Cells with Exogenous Genes of Interest. *Curr. Protoc. Immunol.* 115:1:12. <https://doi.org/10.1002/cpim.15>
- Matute, J.D., A.A. Arias, M.C. Dinauer, and P.J. Patiño. 2005. p40phox: the last NADPH oxidase subunit. *Blood Cells Mol. Dis.* 35:291–302. <https://doi.org/10.1016/j.bcmd.2005.06.010>
- Matute, J.D., A.A. Arias, N.A.M. Wright, I. Wrobel, C.C.M. Waterhouse, X.J. Li, C.C. Marchal, N.D. Stull, D.B. Lewis, M. Steele, et al. 2009. A new genetic subgroup of chronic granulomatous disease with autosomal recessive mutations in p40 phox and selective defects in neutrophil NADPH oxidase activity. *Blood*. 114:3309–3315. <https://doi.org/10.1182/blood-2009-07-231498>
- Mecklenbräuer, I., S.L. Kalled, M. Leitges, F. Mackay, and A. Tarakhovskiy. 2004. Regulation of B-cell survival by BAFF-dependent PKCdelta-mediated nuclear signalling. *Nature*. 431:456–461. <https://doi.org/10.1038/nature02955>
- Mecklenbräuer, I., K. Saijo, N.-Y. Zheng, M. Leitges, and A. Tarakhovskiy. 2002. Protein kinase Cdelta controls self-antigen-induced B-cell tolerance. *Nature*. 416:860–865. <https://doi.org/10.1038/416860a>
- Meffre, E., and H. Wardemann. 2008. B-cell tolerance checkpoints in health and autoimmunity. *Curr. Opin. Immunol.* 20:632–638. <https://doi.org/10.1016/j.coi.2008.09.001>
- Meijles, D.N., L.M. Fan, B.J. Howlin, and J.-M. Li. 2014. Molecular insights of p47phox phosphorylation dynamics in the regulation of NADPH oxidase activation and superoxide production. *J. Biol. Chem.* 289:22759–22770. <https://doi.org/10.1074/jbc.M114.561159>
- Meyts, I., G. Bucciol, I. Quinti, B. Neven, A. Fischer, E. Seoane, E. Lopez-Granados, C. Gianelli, A. Robles-Marhuenda, P.Y. Jeandel, et al. IUIS Committee of Inborn Errors of Immunity. 2021. Coronavirus disease 2019 in patients with inborn errors of immunity: An international study. *J. Allergy Clin. Immunol.* 147:520–531. <https://doi.org/10.1016/j.jaci.2020.09.010>
- Miyamoto, A., K. Nakayama, H. Imaki, S. Hirose, Y. Jiang, M. Abe, T. Tsukiyama, H. Nagahama, S. Ohno, S. Hatakeyama, and K.I. Nakayama. 2002. Increased proliferation of B cells and auto-immunity in mice lacking protein kinase Cdelta. *Nature*. 416:865–869. <https://doi.org/10.1038/416865a>
- Nanthapaisal, S., E. Omoyinmi, C. Murphy, A. Standing, M. Eisenhut, D. Eleftheriou, and P.A. Brogan. 2017. Early-Onset Juvenile SLE Associated With a Novel Mutation in Protein Kinase C δ. *Pediatrics*. 139:e20160781. <https://doi.org/10.1542/peds.2016-0781>
- Neehus, A.-L., J. Lam, K. Haake, S. Merkert, N. Schmidt, A. Mucci, M. Ackermann, M. Schubert, C. Happle, M.P. Kühnel, et al. 2018. Impaired IFNγ-Signaling and Mycobacterial Clearance in IFNγR1-Deficient Human iPSC-Derived Macrophages. *Stem Cell Reports*. 10:7–16. <https://doi.org/10.1016/j.stemcr.2017.11.011>
- Newton, A.C. 2001. Protein kinase C: structural and spatial regulation by phosphorylation, cofactors, and macromolecular interactions. *Chem. Rev.* 101:2353–2364. <https://doi.org/10.1021/cr0002801>
- Nishikawa, K., A. Toker, F.-J. Johannes, Z. Songyang, and L.C. Cantley. 1997. Determination of the specific substrate sequence motifs of protein kinase C isozymes. *J. Biol. Chem.* 272:952–960. <https://doi.org/10.1074/jbc.272.2.952>
- Nishizuka, Y. 1995. Protein kinase C and lipid signaling for sustained cellular responses. *FASEB J.* 9:484–496. <https://doi.org/10.1096/fasebj.9.7.7737456>
- Norouzi, S., A. Aghamohammadi, S. Mamishi, S.D. Rosenzweig, and N. Rezaei. 2012. Bacillus Calmette-Guérin (BCG) complications associated with primary immunodeficiency diseases. *J. Infect.* 64:543–554. <https://doi.org/10.1016/j.jinf.2012.03.012>
- Omarjee, O., C. Picard, C. Frachette, M. Moreews, F. Rieux-Laucat, P. Soulas-Sprauel, S. Viel, J.-C. Lega, B. Bader-Meunier, T. Walzer, et al. 2019. Monogenic lupus: Dissecting heterogeneity. *Autoimmun. Rev.* 18:102361. <https://doi.org/10.1016/j.autrev.2019.102361>
- Pappa, H., J. Murray-Rust, L.V. Dekker, P.J. Parker, and N.Q. McDonald. 1998. Crystal structure of the C2 domain from protein kinase C-δ. *Structure*. 6:885–894. [https://doi.org/10.1016/S0969-2126\(98\)00090-2](https://doi.org/10.1016/S0969-2126(98)00090-2)
- Parvaneh, V.J., R. Shiari, L. Mahbobi, and D. Babaei. 2014. Chronic granulomatous disease associated with systemic lupus erythematosus and systemic onset juvenile idiopathic arthritis. *Pediatr. Rheumatol.* 12(S1):P169. <https://doi.org/10.1186/1546-0096-12-S1-P169>
- Picard, C., and A. Belot. 2017. Does type-I interferon drive systemic autoimmunity? *Autoimmun. Rev.* 16:897–902. <https://doi.org/10.1016/j.autrev.2017.07.001>

- Rahman, A., and D.A. Isenberg. 2008. Systemic lupus erythematosus. *N. Engl. J. Med.* 358:929–939. <https://doi.org/10.1056/NEJMra071297>
- Reyland, M.E., S.M. Anderson, A.A. Matassa, K.A. Barzen, and D.O. Quissell. 1999. Protein kinase C  $\delta$  is essential for etoposide-induced apoptosis in salivary gland acinar cells. *J. Biol. Chem.* 274:19115–19123. <https://doi.org/10.1074/jbc.274.27.19115>
- Rönblom, L.E., G.V. Alm, and K.E. Oberg. 1990. Possible induction of systemic lupus erythematosus by interferon-alpha treatment in a patient with an inherited human disorder--chronic granulomatous disease--on the basis of its chromosomal location. *Nature.* 322:32–38. <https://doi.org/10.1111/j.1365-2796.1990.tb00144.x>
- Royer-Pokora, B., L.M. Kunkel, A.P. Monaco, S.C. Goff, P.E. Newburger, R.L. Baehner, F.S. Cole, J.T. Curnutte, and S.H. Orkin. 1986. Cloning the gene for an inherited human disorder--chronic granulomatous disease--on the basis of its chromosomal location. *Nature.* 322:32–38. <https://doi.org/10.1038/322032a0>
- Salzer, E., E. Santos-Valente, S. Klaver, S.A. Ban, W. Emminger, N.K. Prengemann, W. Garncarz, L. Müllauer, R. Kain, H. Boztug, et al. 2013. B-cell deficiency and severe autoimmunity caused by deficiency of protein kinase C  $\delta$ . *Blood.* 121:3112–3116. <https://doi.org/10.1182/blood-2012-10-460741>
- Salzer, E., E. Santos-Valente, B. Keller, K. Warnatz, and K. Boztug. 2016. Protein Kinase C  $\delta$ : a Gatekeeper of Immune Homeostasis. *J. Clin. Immunol.* 36:631–640. <https://doi.org/10.1007/s10875-016-0323-0>
- Schwegmann, A., R. Guler, A.J. Cutler, B. Arendse, W.G.C. Horsnell, A. Flemming, A.H. Kottmann, G. Ryan, W. Hide, M. Leitges, et al. 2007. Protein kinase C  $\delta$  is essential for optimal macrophage-mediated phagosomal containment of *Listeria monocytogenes*. *Proc. Natl. Acad. Sci. USA.* 104:16251–16256. <https://doi.org/10.1073/pnas.0703496104>
- Segal, B.H., T.L. Leto, J.I. Gallin, H.L. Malech, and S.M. Holland. 2000. Genetic, biochemical, and clinical features of chronic granulomatous disease. *Medicine (Baltimore).* 79:170–200. <https://doi.org/10.1097/00005792-200005000-00004>
- Sharifinejad, N., G. Azizi, N. Behniafard, M. Zaki-Dizaji, M. Jamee, R. Yazdani, H. Abolhassani, and A. Aghamohammadi. 2020. Protein Kinase C-Delta Defect in Autoimmune Lymphoproliferative Syndrome-Like Disease: First Case from the National Iranian Registry and Review of the Literature. *Immunol. Invest.*:1–12. <https://doi.org/10.1080/08820139.2020.1829638>
- Someya, A., H. Nunoi, T. Hasebe, and I. Nagaoka. 1999. Phosphorylation of p40-phox during activation of neutrophil NADPH oxidase. *J. Leukoc. Biol.* 66:851–857. <https://doi.org/10.1002/jlb.66.5.851>
- Song, E., G.B. Jaishankar, H. Saleh, W. Jithpratuck, R. Sahni, and G. Krishnaswamy. 2011. Chronic granulomatous disease: a review of the infectious and inflammatory complications. *Clin. Mol. Allergy.* 9:10. <https://doi.org/10.1186/1476-7961-9-10>
- Sontag, S., M. Förster, J. Qin, P. Wanek, S. Mitzka, H.M. Schüler, S. Koschmieder, S. Rose-John, K. Seré, and M. Zenke. 2017. Modelling IRF8 Deficient Human Hematopoiesis and Dendritic Cell Development with Engineered iPS Cells. *Stem Cells.* 35:898–908. <https://doi.org/10.1002/stem.2565>
- Soroush, F., Y. Tang, K. Guglielmo, A. Engelmann, E. Liverani, A. Patel, J. Langston, S. Sun, S. Kunapuli, M.F. Kiani, and L.E. Kilpatrick. 2019. Protein Kinase C-Delta (PKC $\delta$ ) Tyrosine Phosphorylation is a Critical Regulator of Neutrophil-Endothelial Cell Interaction in Inflammation. *Shock.* 51:538–547. <https://doi.org/10.1097/SHK.0000000000001247>
- Szilagyi, K., R.P. Gazendam, J.L. van Hamme, A.T.J. Tool, M. van Houdt, W.A.J.W. Vos, P. Verkuijlen, H. Janssen, A. Belot, L. Juillard, et al. 2015. Impaired microbial killing by neutrophils from patients with protein kinase C delta deficiency. *J. Allergy Clin. Immunol.* 136:1404–7.e1: 10. <https://doi.org/10.1016/j.jaci.2015.06.016>
- Thomas, D.C., L.-M. Charbonnier, A. Schejtman, H. Aldhekri, E.L. Coomber, E.R. Dufficy, A.E. Beenken, J.C. Lee, S. Clare, A.O. Speak, et al. 2019. EROS/CYBC1 mutations: Decreased NADPH oxidase function and chronic granulomatous disease. *J. Allergy Clin. Immunol.* 143:782–785.e1. <https://doi.org/10.1016/j.jaci.2018.09.019>
- van de Geer, A., A. Nieto-Patlán, D.B. Kuhns, A.T.J. Tool, A.A. Arias, M. Bouazziz, M. de Boer, J.L. Franco, R.P. Gazendam, J.L. van Hamme, et al. 2018. Inherited p40<sup>phox</sup> deficiency differs from classic chronic granulomatous disease. *J. Clin. Invest.* 128:3957–3975. <https://doi.org/10.1172/JCI97116>
- Winkelstein, J.A., M.C. Marino, R.B. Johnston Jr., J. Boyle, J. Curnutte, J.I. Gallin, H.L. Malech, S.M. Holland, H. Ochs, P. Quie, et al. 2000. Chronic granulomatous disease. Report on a national registry of 368 patients. *Medicine (Baltimore).* 79:155–169. <https://doi.org/10.1097/00005792-200005000-00003>
- Wright, M., S. Chandrakasan, D.T. Okou, H. Yin, I. Jurickova, L.A. Denson, and S. Kugathasan. 2019. Early Onset Granulomatous Colitis Associated with a Mutation in NCF4 Resolved with Hematopoietic Stem Cell Transplantation. *J. Pediatr.* 210:220–225. <https://doi.org/10.1016/j.jpeds.2019.03.042>
- Wu-Zhang, A.X., A.N. Murphy, M. Bachman, and A.C. Newton. 2012. Isozyme-specific interaction of protein kinase C $\delta$  with mitochondria dissected using live cell fluorescence imaging. *J. Biol. Chem.* 287:37891–37906. <https://doi.org/10.1074/jbc.M112.412635>
- Xie, C., T. Cole, C. McLean, and J.C. Su. 2016. Association Between Discoid Lupus Erythematosus and Chronic Granulomatous Disease--Report of Two Cases and Review of the Literature. *Pediatr. Dermatol.* 33:e114–e120. <https://doi.org/10.1111/pde.12826>
- Yang, Q., J.C. Langston, Y. Tang, M.F. Kiani, and L.E. Kilpatrick. 2019. The Role of Tyrosine Phosphorylation of Protein Kinase C Delta in Infection and Inflammation. *Int. J. Mol. Sci.* 20:1498. <https://doi.org/10.3390/ijms20061498>
- Zhang, G., M.G. Kazanietz, P.M. Blumberg, and J.H. Hurley. 1995. Crystal structure of the cys2 activator-binding domain of protein kinase C delta in complex with phorbol ester. *Cell.* 81:917–924. [https://doi.org/10.1016/0092-8674\(95\)90011-X](https://doi.org/10.1016/0092-8674(95)90011-X)
- Zhao, X., B. Xu, A. Bhattacharjee, C.M. Oldfield, F.B. Wientjes, G.M. Feldman, and M.K. Cathcart. 2005. Protein kinase Cdelta regulates p67phox phosphorylation in human monocytes. *J. Leukoc. Biol.* 77:414–420. <https://doi.org/10.1189/jlb.0504284>

## Supplemental material



Downloaded from [http://rupress.org/jem/article-pdf/218/9/e20210501/1419330/jem\\_20210501.pdf](http://rupress.org/jem/article-pdf/218/9/e20210501/1419330/jem_20210501.pdf) by Uci Library Services user on 28 July 2021

Figure S1. **Evolutionary conservation of PKC $\delta$  and PRKCD transcripts in cells carrying essential splice site variants.** (A) Amino-acid residue conservation in various species, for the four PKC $\delta$  missense mutations (indicated by red arrows) found in kindreds A–D. (B) Schematic diagram and proportions of the different splice variants produced in cells from homozygous carriers of the c.1352 + 1G>A or c.517 + 2dup variants and compound heterozygous carriers of the p.Q191\* and c.788-2A>G variants. Positions of affected amino acids are indicated by red triangles.

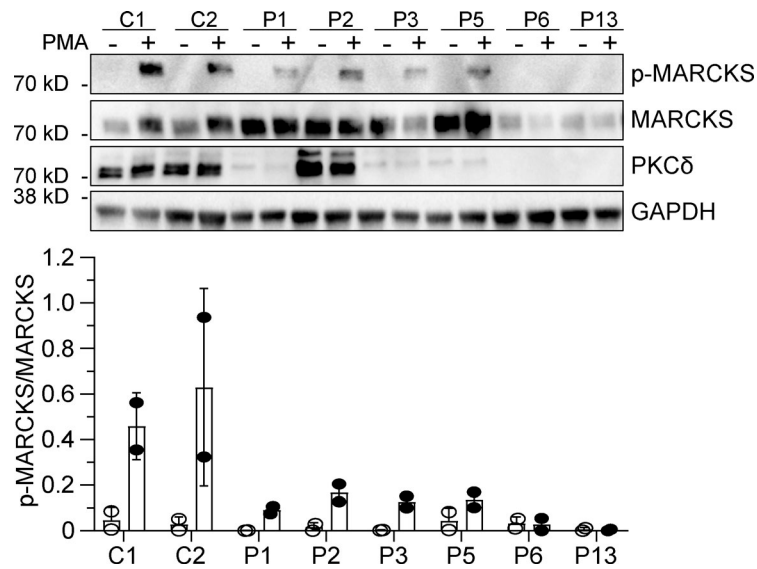
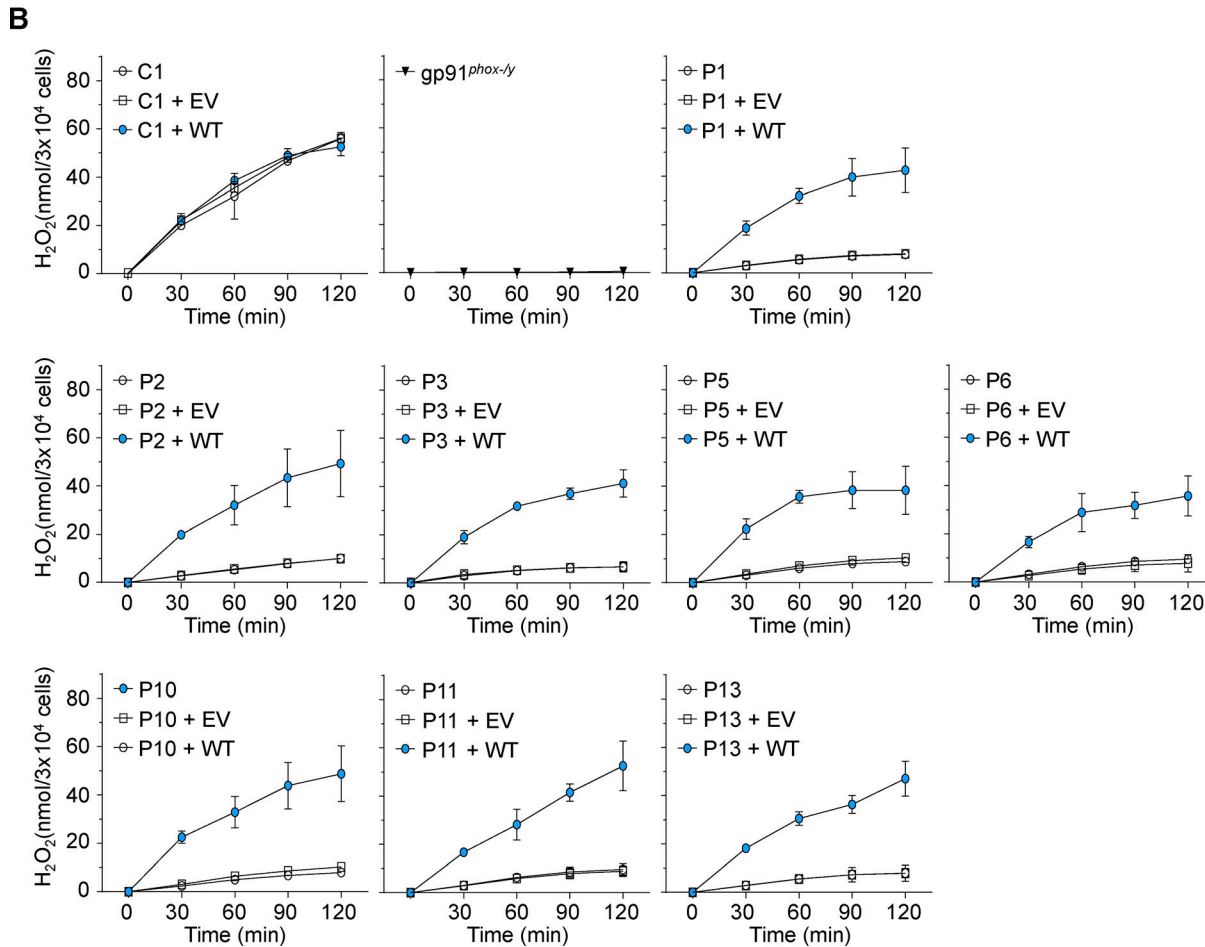
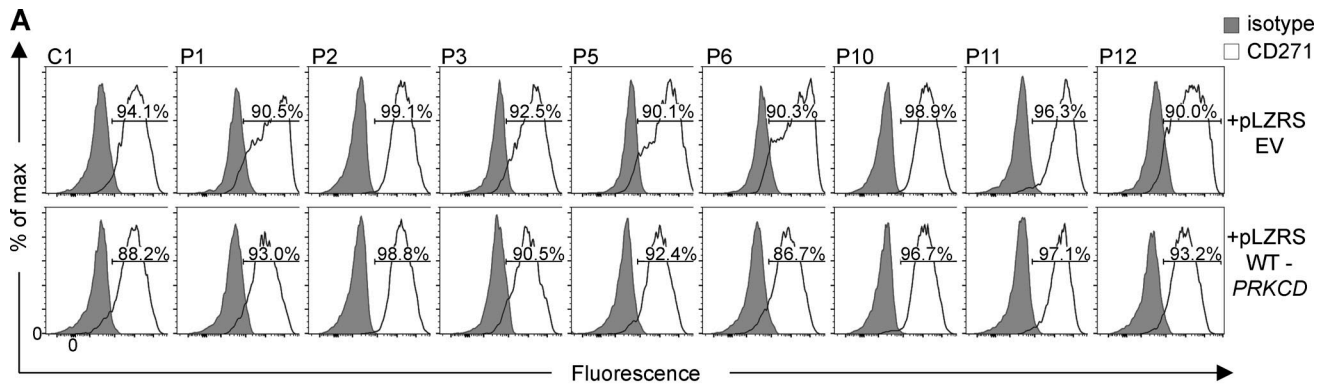


Figure S2. **Phosphorylation of MARCKS in the patients' EBV-B cells.** Phosphorylation of MARCKS was detected by Western blot using whole-cell protein lysates of EBV-B cells of two healthy controls (C1, C2) and PKC $\delta$ -deficient patients before (-) and after (+) 30-min PMA activation (upper panel; 400 ng/ml). Antibodies against phospho-MARCKS (p-MARCKS), MARCKS, and PKC $\delta$  were used. An antibody against GAPDH was used as loading control. Quantification of pMARCKS expression compared with the amount of total MARCKS (lower panel;  $n = 2$ ; mean  $\pm$  SD). The results shown are representative of two independent experiments.



**Figure S3. Complementation of the patients' EBV-B cells with WT PRKCD. (A)** Surface expression of CD271 on EBV-B cells of a healthy control (C1) and PKC $\delta$ -deficient patients after retroviral transduction with the empty pLZRS vector (EV) and WT PRKCD cDNA (gray, isotype; black, surface staining). **(B)** Extracellular H<sub>2</sub>O<sub>2</sub> production by the EBV-B cells of a healthy control (C1), a gp91<sup>phox-ly</sup>-deficient patient, and PKC $\delta$ -deficient patients either nontransduced (NT) or transduced with the empty pLZRS plasmid (EV) or WT-PRKCD, at various time points after PMA stimulation (400 ng/ml), as assessed with the Amplex Red test. Representative results of two independent experiments (duplicates, mean  $\pm$  SD).

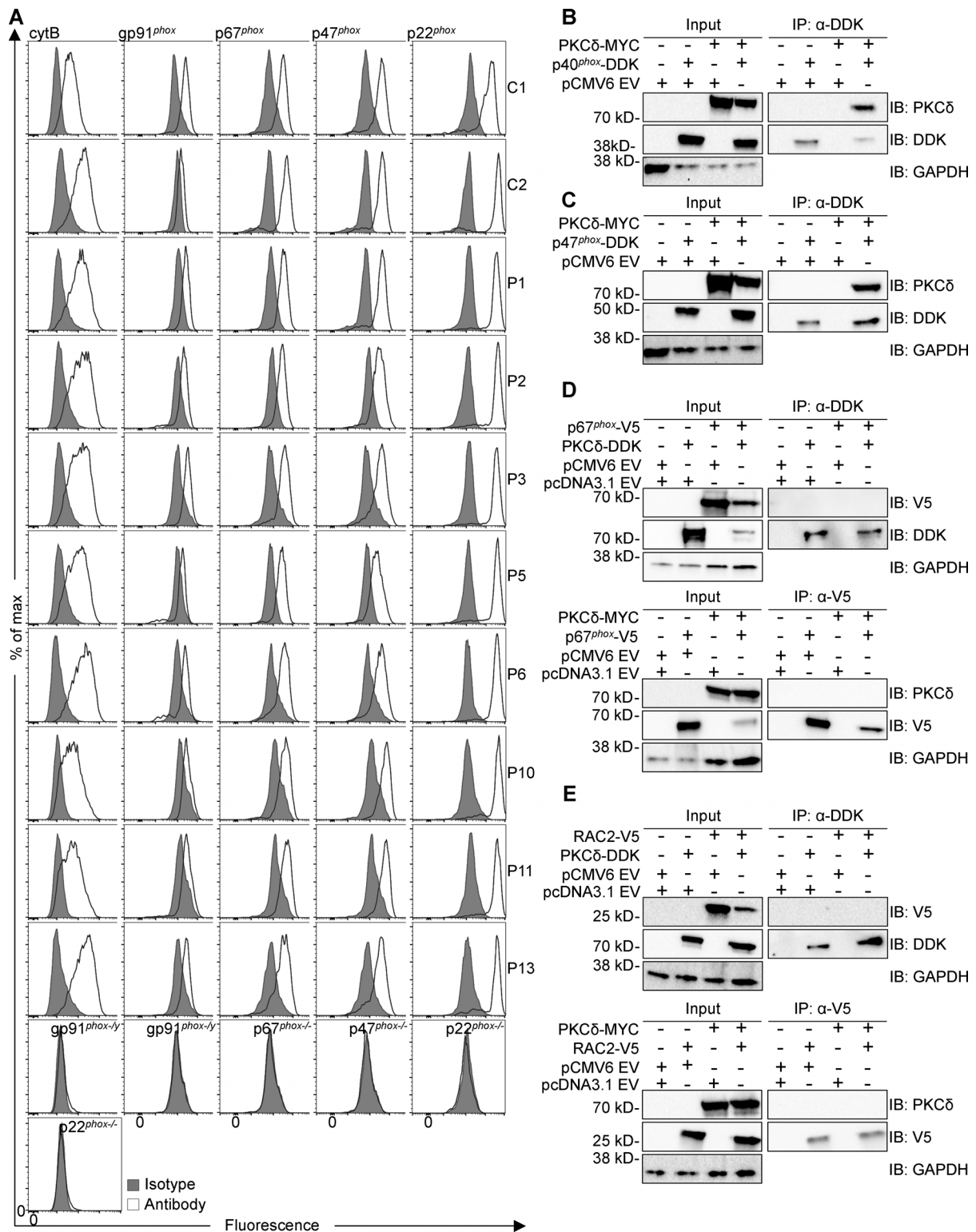


Figure S4. **Expression of NADPH oxidase components in PKC $\delta$ -deficient EBV-B cells and their interaction with PKC $\delta$ .** (A) Extracellular detection of cytochrome *b*<sub>558</sub> (cytB) and intracellular staining for gp91<sup>phox</sup>, p67<sup>phox</sup>, p47<sup>phox</sup>, and p22<sup>phox</sup> in EBV-B cells from healthy controls (C1, C2), PKC $\delta$ -deficient patients, and CGD patients (gray, isotype; black, surface staining). Representative results are shown for three independent experiments. (B) Coimmunoprecipitation (IP) on protein lysates from HEK293T cells transfected with the empty vector (EV), *NCF4*, or *PRKCD* cDNAs. The pull-down of p40<sup>phox</sup> was performed with an anti-DDK antibody. (C) IP on protein lysates from HEK293T cells transfected with EV, *NCF1*, or *PRKCD* cDNAs. The pull-down of p47<sup>phox</sup> was performed with an anti-DDK antibody. (D) Co-IP on protein lysates from HEK293T cells transfected with EV, *NCF2*, or *PRKCD* cDNAs. The pull-down of PKC $\delta$  (upper panel) and p67<sup>phox</sup> (lower panel) was performed with an anti-DDK or an anti-V5 antibody, respectively. (E) IP on protein lysates from HEK293T cells transfected with EV, *RAC2*, or *PRKCD* cDNAs. The pull-down of PKC $\delta$  (upper panel) and Rac2 (lower panel) was performed with an anti-DDK or an anti-V5 antibody, respectively. All results shown are representative of two independent experiments.

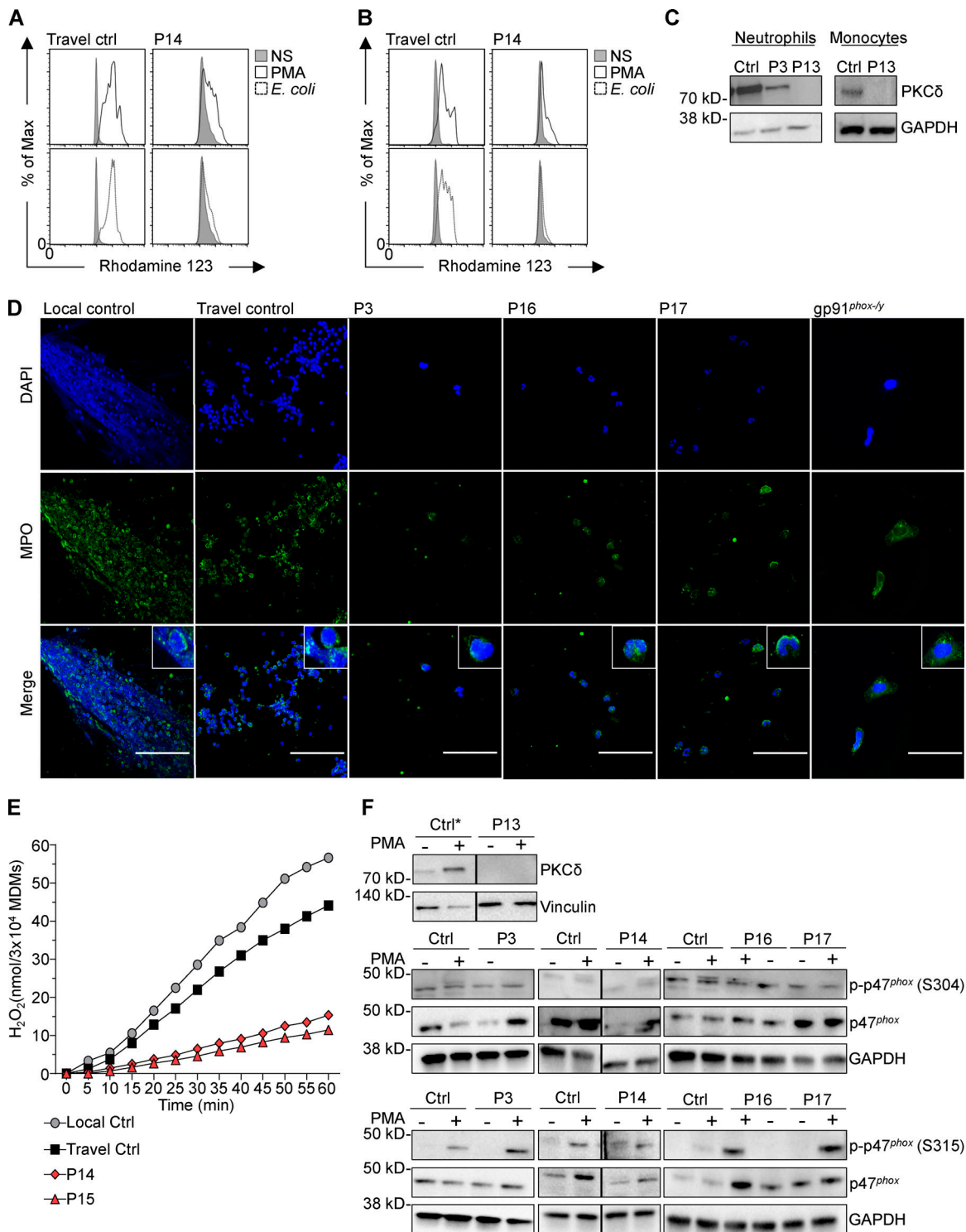


Figure S5. **NADPH oxidase activity and p47<sup>phox</sup> phosphorylation in primary cells of PKC $\delta$ -deficient patients.** (A and B) Representative flow cytometry images of intracellular ROS production measured by DHR in neutrophils (A) and monocytes (B) of a healthy control and a PKC $\delta$ -deficient patient (P14) are shown on the right (gray filled, nonstimulated; black solid line, PMA stimulation; black dotted line, *E. coli* stimulation). (C) PKC $\delta$  expression in neutrophils and monocytes of healthy controls and two PKC $\delta$ -deficient patients, measured by Western blot. (D) Representative images of PMA-induced NET formation by neutrophils of controls, three PKC $\delta$ -deficient patients, and a gp91<sup>phox-ly</sup>-deficient patient. Green represents myeloperoxidase (MPO) and blue DNA (DAPI). The merged images of the local and travel controls and of P17 are the same as displayed in Fig. 7 C. Scale bars, 60  $\mu$ m. (E) Representative kinetic of extracellular H<sub>2</sub>O<sub>2</sub> production after PMA plus IFN- $\gamma$  stimulation by MDMs of patients (P14, P15) and controls. (F) Western Blot of MDMs of healthy controls (n = 4) and PKC $\delta$ -deficient patients (n = 5) before (-) and after (+) 30 min of PMA stimulation (400 ng/ml). Antibodies against PKC $\delta$ , phosphoS304-p47<sup>phox</sup>, phosphoS315-p47<sup>phox</sup>, and p47<sup>phox</sup> were used. Anti-GAPDH and anti-Vinculin antibodies served as a loading controls. The control marked with an asterisk is the same as in Fig. 7 D because proteins of P2 (Fig. 7 D) and P13 were blotted on the same membrane. Solid bars between two images indicate different regions of the same membrane.

Provided online are three tables. Table S1 lists primer sequences and conditions for genomic amplification of the *PRKCD* gene. Table S2 lists primer sequences for site-directed mutagenesis using the pCMV6-*PRKCD*-WT-DDK plasmid. Table S3 lists antibodies used.